OXFORD UNIVERSITY PRESS | Mathematical Medicine and Biology: A Journal of the IMA

A model of strongly-biased chemotaxis reveals the tradeoffs of different bacterial migration strategies.

Journal:	*Mathematical Medicine and Biology: A Journal of the IMA*
Manuscript ID	MMB-18-045.R2
Manuscript Type:	Original Manuscripts
Date Submitted by the Author:	n/a
Complete List of Authors:	Bearon, Rachel; University of Liverpool, Mathematical Sciences Durham, William; University of Sheffield, Department of Physics and Astronomy
Keywords:	bacteria, chemotaxis, biofilms, PDEs, stochastic simulations
Note: The following files were submitted by the author for peer review, but cannot be converted to PDF. You must view these files (e.g. movies) online.	
Production.zip	

Mathematical Medicine and Biology Page 1 of 36
doi:10.1093/imammb/dqnxxx

A model of strongly-biased chemotaxis reveals the tradeoffs of different bacterial migration strategies.

R. N. BEARON
Department of Mathematical Sciences, University of Liverpool, Liverpool, L69 7ZL, UK.

W. M. DURHAM
Department of Physics and Astronomy, University of Sheffield, Sheffield, S3 7RH, UK

[Received: date / Accepted: date]

Many bacteria actively bias their motility towards more favourable nutrient environments. In liquid, cells rotate their corkscrew shaped flagella to swim, but in surface attached biofilms cells instead use grappling hook like appendages called pili to pull themselves along. In both forms of motility cells selectively alternate between relatively straight 'runs' and sharp reorientations to generate biased random walks up chemoattractant gradients. However, recent experiments suggest that swimming and biofilm cells employ fundamentally different strategies to generate chemotaxis: swimming cells typically suppress reorientations when moving up a chemoattractant gradient, whereas biofilm cells increase reorientations when moving down a chemoattractant gradient. The reason for this difference remains unknown. Here we develop a mathematical framework to understand how these different chemotactic strategies affect the distribution of cells at the population level. Current continuum models typically assume a weak bias in the reorientation rate and are not able to distinguish between these two strategies, so we derive a model for strong chemotaxis which resolves how both the drift and diffusive components depend on the underlying chemotactic strategy. We then test predictions from our continuum model against individual-based simulations, and identify further refinements that allow our continuum model to resolve boundary effects. Our analyses reveal that the strategy employed by swimming cells yields a larger chemotactic drift, but the strategy used by biofilm cells allows them to more tightly aggregate where the chemoattractant is most abundant. This new modelling framework provides new quantitative insights into how the different chemical landscapes experienced by swimming and biofilm cells might select for divergent ways of generating chemotaxis.

Keywords: bacteria; chemotaxis; biofilms; PDEs; stochastic simulations

1. Introduction

Bacteria are among the most primitive forms of life. Yet, despite their relative simplicity and small size (≈ 1 to $100\mu m$), bacteria can actively sense a remarkable diversity of different environmental signals, including light, temperature, pH, oxygen, nutrients, and toxins, and use this information to direct their motility towards more favourable environments. While not all bacterial species are motile, bacterial motility plays a vital role in many processes in both nature and medicine. For example, bacteria's ability to bias their movement along chemical gradients increases the productivity of the marine ecosystems (Smirga *et al.*, 2016), enhances the degradation of pollutants (Pandey & Jain, 2002), and localises potentially fatal cholera infections to a certain part of the gut (Butler & Camili, 2005). This process, known as chemotaxis, is widely studied and the enteric bacteria *Escherichia coli* serves as a model system in

the study of bacterial chemotaxis. Over the last four decades tremendous progress has been made in characterising the underlying biophysical processes that *E. coli* cells use to navigate chemical gradients, from how the different proteins in the signal transduction pathway function (Berg, 2004; Wadhams & Armitage, 2004), to how its multiple flagella interact hydrodynamically (Kim *et al.*, 2003), to how their biased random walks affect cell distributions at the population level (Alt, 1980; Rivero *et al.*, 1989; Hillen & Othmer, 2000; Erban & Othmer, 2005; Othmer & Xue, 2013; Thygesen, 2016; Xue & Yang, 2016).

Swimming bacteria like *E. coli* navigate along gradients by regulating the rotation direction of their corkscrew-like flagella. When they rotate their flagella in one direction the flagella bundle together to move the cell forward in a relatively straight 'run', but when one of the flagella turns the opposite direction the bundle flies apart causing the cell to 'tumble' and sharply change direction. In the absence of external stimuli, *E. coli* cells tumble randomly in time, with a mean duration between successive tumbles of approximately one second. In the presence of a chemical gradient, cells use a finely-tuned chemosensory system to measure changes in the concentration of chemical over time and when a cell senses it is moving up a gradient of nutrient it extends runs. However, when it senses it is traveling down a nutrient gradient it simply reverts back to the basal tumbling rate that it exhibits in the absence of chemical gradients (Berg & Brown, 1972). In this way, *E. coli* is said to have an 'optimistic' chemotactic strategy: if conditions are getting better it keeps going, but if conditions get worse it does nothing (Berg & Brown, 1972; Berg, 2004). While Brownian rotational diffusion randomizes a cell's swimming direction and prevents it from swimming directly up a gradient, this optimistic strategy allows a cell to perform a biased random walk towards more favourable nutrient environments.

The majority of bacteria, however, live in surface attached biofilms where flagella are largely ineffective at driving movement (Costerton *et al.*, 1995). Instead, in these environments bacteria pull themselves across surfaces using grappling hook type appendages known as Type IV pili (Skerker & Berg, 2001). While *E. coli* lacks these pili, it was recently demonstrated that *Pseudomonas aeruginosa*, a pathogenic bacteria species widely used as a model of biofilm formation, can perform chemotaxis while attached to surfaces (Oliveira *et al.*, 2016). By following the movement of thousands of attached *P. aeruginosa* within microfluidic devices, it was shown that these rod-shaped bacteria can actively sense their chemical environment and use this information to selectively reverse direction by pulling themselves from their opposite pole. It was found that cells moving up a gradient reverse direction at the same rate as those in the absence of a gradient, but cells that move down the gradient reverse direction more frequently. Thus, these biofilm cells employ a corrective 'pessimistic' strategy that is the mirror image of the strategy used by swimming *E. coli* cells. In other words, the presence of a chemoattractant gradient tends to decrease the reorientation rate of swimming *E. coli* and tends to increase the reorientation rate of surface attached *P. aeruginosa*. This indicates that evolution might select different chemotactic strategies in swimming and biofilm cells. However, we lack fundamental understanding about how these different strategies would affect a cell's ability to acquire nutrients. Here we develop a mathematical framework to understand how the response of individual cells to chemical stimuli affects their distribution at the population level, allowing us to resolve the trade-offs of these different chemotactic strategies.

Mathematical modelling has long been used as a tool to understand how individual cell behaviour gives rise to chemotaxis. Bacterial chemotaxis is experimentally quantified in two distinct ways: at the microscopic scale, by quantifying the movement of individual cells (Berg & Brown, 1972; Ahmed & Stocker, 2008; Oliveira *et al.*, 2016) or at the macroscopic scale, for example, by measuring the size of the rings that form around colonies growing in agar (Adler, 1966; Kearns *et al.*, 2001; Berg, 2004). The Keller-Segel model for chemotaxis, a drift-diffusion partial differential equation model (Keller &

Segel, 1971; Hillen & Painter, 2009), has proved particularly useful for reconciling these two types of experiments (Ahmed & Stocker, 2008). The classic derivation of this model follows Alt (1980) who applied a singular-perturbation approach with parabolic scaling to analyse a governing equation that describes straight 'runs' interspersed by reorientations. This approach forms the basis for more sophisticated models that include additional processes, for example, biochemical signalling and internal state dynamics (Tindall *et al.*, 2008; Othmer & Xue, 2013; Xue & Yang, 2016). Regardless of the specific implementation, however, this class of mathematical model allows one to directly test whether conceptual descriptions of individual cell behaviour can accurately predict macroscopic distributions.

The singular-perturbation approach as used previously, while powerful, has a number of limitations that can restrict its applicability. When working in two or higher spatial dimensions, the tumble rate bias, which measures the difference in the tumble rate for cells moving up and down a gradient, must be sufficiently small so that it can be modelled as a weak linear function of the chemoattractant gradient (Hillen & Othmer, 2000). This gives rise to a linear relationship between chemotactic drift and chemoattractant gradient and a diffusion rate independent of the gradient. While a one-dimensional model, based on the telegraph equation, has been developed that allows for an arbitrary chemotactic response (Rivero *et al.*, 1989), the methods used to close this system of equations cannot easily be extended to higher dimensions. Recently, Xue & Yang (2016) obtained a system of moment-flux models for bacterial chemotaxis in large signal gradients. They incorporated details of the intracellular signalling which explicitly captures the excitation and adaptation time scales, and obtained a coupled system of moment equations which gives excellent agreement between individual-based simulations even in the presence of large chemoattractant gradients when sufficient moments are included.

An alternative approach which enables the construction of a simple drift-diffusion model for chemotaxis even for large gradients was developed by Thygesen (2016). In that work, the tumble rate is assumed to depend exponentially on the chemical gradient, and it is assumed that the direction of successive run segments are independent thus enabling probabilistic tools associated with renewal-reward processes to be applied. However, this model does not capture 'persistence', which occurs when the direction of subsequent runs are correlated. Hillen (2006) and Hillen & Painter (2013) also considered random walks in the absence of persistence, and demonstrated, using a hyperbolic scaling, that a strongly biased random walk model could be described by a leading order drift equation with first order correction for diffusion.

Returning to the singular-perturbation approach, which can include the effect of persistence, we show here how the parabolic scaling can be modified to enable it to be applicable to strongly biased chemotaxis, and obtain simple drift-diffusion models for chemotaxis. This is the novel approach detailed in this paper. In the new singular perturbation approach presented here, diffusion is analysed about a reference frame moving with the mean drift of the cells. This approach has been touched upon previously in the context of run-and-tumble chemotaxis in shear flow (Bearon, 2003) and correlated random-walks (Codling *et al.*, 2010) but this paper presents the first comprehensive description of this approach, including a detailed description of the tumble rate and turn kernel.

In section 2 we introduce the governing equation for the distribution of cell position and direction which describes a model for chemotaxis consisting of 'runs' interspersed with reorientation events. We first introduce cells with a bi-directional bias (*bi-bias*), whereby the tumble rate both increases when cells are moving down the gradient and decreases when cells are moving up the gradient. In the case of a strong chemotactic response, we assume the tumble rate depends exponentially on the chemical gradient; whereas for a weak chemotactic response this reduces to a linear function of chemical gradient. We then specify the optimistic and pessimistic strategies to model swimming and biofilm cells as a one-sided modification to the bi-bias strategy. Considering chemotaxis occurring on a two-

dimensional surface, with a steady homogeneous chemical gradient, we review the derivation of the Keller-Segel drift-diffusion equation for the cell concentration via a singular-perturbation approach for weak chemotactic response. Our new approach, appropriate for strongly-biased chemotaxis, is then presented, yielding again a drift-diffusion equation but with a more complex expression for the diffusivity. This drift-diffusion model for strongly-biased chemotaxis including persistence is the first key new result of the paper.

In section 3, we present several new results using our drift-diffusion model. In section 3.1 we show that the drift-diffusion equations obtained for weak chemotaxis are identical for optimists and pessimists, and therefore cannot capture the difference between the two strategies. In section 3.2, we compute the drift and diffusion coefficients as a function of chemotactic strength for the strongly-biased chemotaxis model, and then use this to resolve how the spatial distribution of bacteria in a bounded region evolves over time. We find that both pessimists and optimists have a lower chemotactic drift rate than the bi-biased cells. However, pessimists have a lower diffusion rate than bi-biased cells, which in turn have a lower diffusion rate than optimists. Furthermore, by examining the equilibrium spatial distributions, we show that, for certain values of chemotactic strength, pessimists are better able to aggregate where the chemoattractant is most abundant. In section 3.3 we investigate the impact of directional correlation between runs on the drift and diffusion coefficients. The model can capture both the classic persistence seen in swimming *E. coli*, which are more likely to continue in the same direction after a tumble, and the reorientation strategy observed for surface attached *P. aeruginosa*, which periodically reverse direction. In section 3.4 we demonstrate how the model can be extended to study orthotaxis, which occurs when cells increase their speed when moving up a chemical gradient, which was observed experimentally (Oliveira *et al.*, 2016), and we provide further comparison with the experiments in section 3.5. In section 3.6, we compare the results from the drift-diffusion continuum model with that from an individual-based model. Both models show the same trends for pessimistic and optimistic strategies, however, as the chemotactic strength is increased, we find discrepancies between the individual-based simulations and solutions of the drift-diffusion model, which are caused by boundary effects. This is explored mathematically, and an alternative analytic equilibrium solution is obtained which agrees well with the individual-based simulations.

2. Model

2.1 *Conservation equation for* $\psi(\boldsymbol{x}^*, \boldsymbol{p}, t^*)$

Our starting point is a conservation equation for the probability distribution function $\psi(\boldsymbol{x}^*, \boldsymbol{p}, t^*)$ representing the distribution of cells with position $\boldsymbol{x}^*$ and direction of movement $\boldsymbol{p}$ at time t^*. Hereinafter, asterisks are used to distinguish dimensional quantities from the dimensionless equivalents. Assuming a Poisson process, in that the turn rate is independent of the run time, from Alt (1980) we obtain a description for run-and-tumble motion:

$$\frac{\partial \psi}{\partial t^*} + \nabla_{\boldsymbol{x}^*} \cdot (V_s \boldsymbol{p} \psi) + \lambda^* \psi - \int_\Omega \lambda^*(\boldsymbol{p}') K(\boldsymbol{p}, \boldsymbol{p}') \psi(\boldsymbol{p}') d\boldsymbol{p}' = 0, \tag{2.1}$$

where functions are assumed to be evaluated at $(\boldsymbol{x}^*, \boldsymbol{p}, t^*)$ unless otherwise stated. The direction of movement before and after tumbles, $\boldsymbol{p}'$ and $\boldsymbol{p}$, are unit vectors, and so the cell velocity is given by $V_s \boldsymbol{p}$. The third term models cells that tumble away from direction $\boldsymbol{p}$ with frequency $\lambda^*(\boldsymbol{p})$ and the fourth term represents cells that tumble from direction $\boldsymbol{p}'$ with frequency $\lambda^*(\boldsymbol{p}')$ and choose a new direction $\boldsymbol{p}$ with probability $K(\boldsymbol{p}, \boldsymbol{p}')$. We note that $\int_\Omega K(\boldsymbol{p}, \boldsymbol{p}') d\boldsymbol{p} = 1$. This parameterization is consistent with the

observation that swimming bacteria measure temporal changes in chemical concentration and use this to modulate their tumble frequency (Berg & Brown, 1972).

2.2 *Chemotactic strategies*

Following Thygesen (2016), we consider a classic model for chemotaxis based on observations of *E. coli* (Brown & Berg, 1974). The logarithm of mean run time is increased proportional to the time rate of change in the number of receptors binding attractant. Assuming the receptor dynamics are at steady state, and that chemoattractant gradient is constant in time, this can be written as

$$\lambda^* = \lambda_0 \exp(-\zeta V_s \boldsymbol{p} \cdot \boldsymbol{\nabla} s), \tag{2.2}$$

where λ_0 is the tumble rate in the absence of chemical gradient, s is the chemoattractant concentration and ζ is proportional to $K_D/(K_D+s)^2$, where K_D is the dissociation constant. For mathematical simplicity, we shall make the approximation that ζ and $\boldsymbol{\nabla} s$ are constant. This parameterization assumes that cells both reduce their tumble rate if moving up a chemical gradient and increase their tumble rate if moving down a chemical gradient. We, therefore, will hereafter call this the bi-directional bias (or *bi-bias*) chemotactic strategy.

Provided $\zeta V_s \boldsymbol{p} \cdot \boldsymbol{\nabla} s \ll 1$, which corresponds to a weak chemotactic response, one can use the linear approximation

$$\lambda^* = \lambda_0 (1 - \zeta V_s \boldsymbol{p} \cdot \boldsymbol{\nabla} s). \tag{2.3}$$

Previous studies that used a singular perturbation derivation to characterize chemotaxis as a drift-diffusion process have all assumed this weak, linear response.

We will also consider optimistic and pessimistic strategies to generate chemotaxis. For optimists, the tumble rate is reduced if moving up a chemical gradient, but unchanged if moving down the gradient:

$$\lambda^* = \lambda_0 \exp(-\zeta V_s (\boldsymbol{p} \cdot \boldsymbol{\nabla} s) H(\boldsymbol{p} \cdot \boldsymbol{\nabla} s)), \tag{2.4}$$

where H is the Heaviside function; equal to one when cells are moving up the gradient, $\boldsymbol{p} \cdot \boldsymbol{\nabla} s > 0$ and zero otherwise. For pessimists, the tumble rate is increased if moving down a chemical gradient, but unchanged if moving up the gradient:

$$\lambda^* = \lambda_0 \exp(-\zeta V_s (\boldsymbol{p} \cdot \boldsymbol{\nabla} s) H(-\boldsymbol{p} \cdot \boldsymbol{\nabla} s)). \tag{2.5}$$

In Table 1 we summarize all parameters and variables considered in the chemotactic model.

2.3 *Chemotaxis on a surface*

Motivated by experiments on surface attached bacteria undergoing chemotaxis (Oliveira *et al.*, 2016), we now restrict attention to the case of cells constrained to a two-dimensional plane, with steady, homogeneous chemical gradient in the positive y^* direction. We define the direction vector in terms of the angle θ:

$$\boldsymbol{p} = \cos\theta \boldsymbol{i} + \sin\theta \boldsymbol{j}. \tag{2.6}$$

If we consider cells uniformly distributed in the x^* direction, the governing equation for $\psi(y^*, \theta, t^*)$ is given by

$$\frac{\partial \psi}{\partial t^*} + \frac{\partial}{\partial y^*}(V_s \sin\theta \psi) + \lambda^* \psi - \int_{-\pi}^{\pi} \lambda^*(\theta') K(\theta, \theta') \psi(\theta') d\theta' = 0. \tag{2.7}$$

Table 1. Key parameters and variables in the chemotactic model

$\psi(\boldsymbol{x},\boldsymbol{p},t)$	Probability distribution of cell position and orientation
$\boldsymbol{p}=\cos\theta\boldsymbol{i}+\sin\theta\boldsymbol{j}$	Direction of movement
$n(y,t)=\int_{-\pi}^{\pi}\psi(y,\theta,t)d\theta$	Probability distribution of cell position
V_s	Cell speed
λ_0	Basal tumble rate
$K(\theta,\theta')=\frac{1}{2\pi I_0(\kappa)}\exp(\kappa\cos(\theta-\theta'))$	Turn kernel, typically Von-Mises distribution with parameter κ; $\kappa=0$ corresponds to isotropic tumbles
$\varepsilon=\frac{V_s}{L\lambda_0}\ll 1$	Ratio of mean basal run length to characteristic length-scale, L
χ	Chemotactic strength, defined following equations (2.2,2.15)
D	Non-dimensional diffusion coefficient
$\overline{p_y}$	Mean component of cell direction up the chemical gradient; $\overline{p_y}=1$ for cells moving purely up the chemical gradient, $\overline{p_y}=0$ for cells moving in random directions

For a steady, homogeneous chemical gradient in the y^* direction, the tumble rate, eq. (2.2), reduces to

$$\lambda^*=\lambda_0\exp(-\zeta V_s\sin\theta\frac{ds}{dy^*}), \tag{2.8}$$

with corresponding linear approximation:

$$\lambda^*=\lambda_0(1-\zeta V_s\sin\theta\frac{ds}{dy^*}). \tag{2.9}$$

The optimistic and pessimistic strategies are given by:

$$\lambda^*_{op} = \lambda_0\exp(-\zeta V_s\sin\theta\frac{ds}{dy^*}H(\sin\theta)), \tag{2.10}$$

$$\lambda^*_{pess} = \lambda_0\exp(-\zeta V_s\sin\theta\frac{ds}{dy^*}H(-\sin\theta)). \tag{2.11}$$

We shall only consider reorientation kernels symmetric in $\theta-\theta'$, i.e.

$$K(\theta,\theta')=h(|\theta-\theta'|), \tag{2.12}$$

where h is an arbitrary smooth function.

2.4 *Formal perturbation approach to derive drift-diffusion model*

To observe diffusive-like behaviour, we need to examine dynamics occurring on length and time scales large compared to typical runs. Furthermore, we use non-dimensionsalization to reduce the number of tunable parameters, a technique used across many different fields (e.g. Leal, 2007). We non-dimensionalise on a characteristic length scale L, such that $y=y^*/L$. This characteristic length scale

can be taken to be the size of the experimental system (Alt, 1980) or the distance over which the cell concentration changes, and define

$$\varepsilon = \frac{V_s}{L\lambda_0} \ll 1. \tag{2.13}$$

This limit of $\varepsilon \ll 1$ corresponds to a situation in which the lengthscale of the variation in the distribution of cells is large compared to a typical run length, $\frac{V_s}{\lambda_0}$. Furthermore we non-dimensionalise time, $t = t^*/T$, based on the time for diffusion to act over the length scale L: $T = L^2\lambda_0/V_s^2 = 1/(\varepsilon^2\lambda_0)$. We thus focus on temporal dynamics that occur on diffusive time scales which are very large compared to the typical run duration, $1/\lambda_0$. More information on this parabolic limit, and also the hyperbolic limit (where instead the time scale is given by $T = 1/(\varepsilon\lambda_0)$) is given by Hillen (2006).

The non-dimensional governing equation for ψ is then given by

$$\varepsilon^2\frac{\partial\psi}{\partial t} + \varepsilon\frac{\partial}{\partial y}(\sin\theta\psi) + \lambda\psi - \int_{-\pi}^{\pi}\lambda(\theta')K(\theta,\theta')\psi(\theta')d\theta' = 0, \tag{2.14}$$

where the tumble rate λ for bi-biased cells is given by

$$\lambda = \exp(-\varepsilon\chi\sin\theta), \tag{2.15}$$

and $\chi = \lambda_0\zeta\frac{ds}{dy}$ measures the chemotactic strength. The corresponding linear approximation is given by

$$\lambda = 1 - \varepsilon\chi\sin\theta. \tag{2.16}$$

This approximation is valid provided $\varepsilon\chi \ll 1$. As we are assuming $\varepsilon \ll 1$ in this perturbation approach, we can use this linear approximation provided $\chi = O(1)$.

The optimistic and pessimistic strategies are given by:

$$\lambda_{op} = \exp(-\varepsilon\chi\sin\theta H(\sin\theta)), \tag{2.17}$$

$$\lambda_{pess} = \exp(-\varepsilon\chi\sin\theta H(-\sin\theta)). \tag{2.18}$$

2.4.1 *Weak chemotaxis* We here review the parabolic scaling approach to obtaining the Keller-Segel drift-diffusion equation for chemotaxis. For a more formal functional analysis approach, the reader is referred for example to Hillen & Othmer (2000) or Othmer & Xue (2013). For weak chemotaxis, with dimensional turn rate given by eq. (2.16), the non-dimensional governing equation for ψ is given by

$$\varepsilon^2\frac{\partial\psi}{\partial t} + \varepsilon\frac{\partial}{\partial y}(\sin\theta\psi) + (1-\varepsilon\chi\sin\theta)\psi - \int_{-\pi}^{\pi}(1-\varepsilon\chi\sin\theta')K(\theta,\theta')\psi(\theta')d\theta' = 0. \tag{2.19}$$

To obtain a closed equation for the cell concentration, $n(y,t)$, we first define the first three moments of ψ:

$$n(y,t) = \int_{-\pi}^{\pi}\psi(y,\theta,t)d\theta, \tag{2.20}$$

$$j(y,t) = \int_{-\pi}^{\pi}\sin\theta\psi d\theta, \tag{2.21}$$

$$Q(y,t) = \int_{-\pi}^{\pi}\sin^2\theta\psi d\theta. \tag{2.22}$$

Taking moments of equation (2.19) yields equations relating these moments (see appendix B, using the approach reviewed for example by Saintillan & Shelley (2013)):

$$\varepsilon^2 \frac{\partial n}{\partial t} + \varepsilon \frac{\partial j}{\partial y} = 0, \tag{2.23}$$

$$\varepsilon^2 \frac{\partial j}{\partial t} + \varepsilon \frac{\partial Q}{\partial y} + (1-\alpha) j - \varepsilon(1-\alpha)\chi Q = 0, \tag{2.24}$$

where α is the index of persistence (Lovely & Dahlquist, 1975; Othmer & Xue, 2013) measuring the mean cosine of the turn angle (i.e. the mean angle between two consecutive runs, see appendix A). To close the system, we now make use of the fact that $\varepsilon \ll 1$ and consider a perturbation expansion for ψ:

$$\psi = \psi^{(0)}(y,\theta,t) + \varepsilon \psi^{(1)}(y,\theta,t) + \cdots. \tag{2.25}$$

At leading order, from equation (2.19) we have that

$$\psi^{(0)} = \int_{-\pi}^{\pi} K(\theta,\theta')\psi^{(0)}(\theta')d\theta'. \tag{2.26}$$

For the class of turn kernel given by equation (2.12), this equation has the unique solution

$$\psi^{(0)}(y,\theta,t) = \frac{1}{2\pi} n^{(0)}(y,t). \tag{2.27}$$

A proof of this result is provided in appendix A, for more details see Hillen & Othmer (2000). Intuitively, if the turn kernel only depends on the change in direction, $|\theta - \theta'|$, and allows cells to sample all possible orientations, the isotropic solution will be the leading order equilibrium solution. That is, after sufficient reorientation events, we expect there to be no bias in the orientation distribution at leading order.

We thus have that

$$j^{(0)} = \int_{-\pi}^{\pi} \sin\theta \psi^{(0)} d\theta = 0, \tag{2.28}$$

$$Q^{(0)} = \int_{-\pi}^{\pi} \sin^2\theta \psi^{(0)} d\theta = \frac{1}{2} n^{(0)}(y,t). \tag{2.29}$$

Equations (2.23) and (2.24) thus give

$$\text{At} \quad O(\varepsilon^2): \quad \frac{\partial n^{(0)}}{\partial t} + \frac{\partial j^{(1)}}{\partial y} = 0, \tag{2.30}$$

$$\text{At} \quad O(\varepsilon): \frac{\partial Q^{(0)}}{\partial y} + (1-\alpha) j^{(1)} - (1-\alpha)\chi Q^{(0)} = 0, \tag{2.31}$$

which, on inserting the expression $Q^{(0)} = \frac{1}{2} n^{(0)}(y,t)$, can be rearranged to give a single equation for $n^{(0)}$:

$$\frac{\partial n^{(0)}}{\partial t} + \frac{1}{2}\frac{\partial}{\partial y}\left(\chi n^{(0)} - \frac{1}{(1-\alpha)}\frac{\partial n^{(0)}}{\partial y}\right) = 0. \tag{2.32}$$

To compare with previous results and examine the explicit dependence of chemotactic drift and diffusion on speed and turn rate, it is helpful to write this equation in terms of dimensional quantities:

$$\frac{\partial n^{(0)}}{\partial t^*} + \frac{\partial}{\partial y^*}\left(\frac{1}{2}\varepsilon\chi V_s n^{(0)} - \frac{1}{2(1-\alpha)}\frac{V_s^2}{\lambda_0}\frac{\partial n^{(0)}}{\partial y^*}\right) = 0. \tag{2.33}$$

The chemotactic drift velocity, $\frac{1}{2}\varepsilon\chi V_s = \frac{1}{2}V_s^2\zeta\frac{ds}{dy^*}$, depends quadratically on cell speed, which is in agreement with previous results (e.g. Rivero *et al.*, 1989). In addition, we find that the diffusivity is proportional to $\frac{V_s^2}{\lambda_0}$ as predicted by the classic Keller-Segel model of chemotaxis, with persistence modifying the diffusion co-coefficient in the same way as described by Lovely & Dahlquist (1975). Note that the bias in the tumble rate affects the drift component, but it does not affect the rate of diffusion, as we are only examining the weak, leading-order effects of chemotaxis.

In the case of weak chemotaxis, we can relate the ratio of turn rates up and down the gradient to the drift velocity. For bi-biased cells, we have that

$$\frac{\lambda_{up}}{\lambda_{down}} \approx 1 - 2\varepsilon\chi, \tag{2.34}$$

and so the chemotactic drift is given by

$$\frac{1}{2}\varepsilon\chi V_s \approx \frac{1}{4}(1 - \frac{\lambda_{up}}{\lambda_{down}})V_s. \tag{2.35}$$

For this model of weak chemotaxis, we thus obtain an upper bound of chemotactic drift equivalent to 25% of the cell speed. In contrast, *E. coli* has been observed to attain a chemotactic drift of approximately 30% of its swimming speed under certain conditions (Ahmed & Stocker, 2008). Furthermore, we note that even approaching this theoretical limit of 25% invalidates the assumption of weak chemotaxis as it assumes the ratio of tumble rates tends to zero. Therefore, this formulation clearly cannot be used to model cells that are capable of biasing a large fraction of their motility up a chemical gradient.

2.4.2 *Arbitrary chemotactic response* For strong chemotaxis, we may expect the mean drift to be strong, and so to examine the diffusive behaviour around this, we need to change to a reference frame moving with the mean drift (c.f. Bearon & Grünbaum (2008); Codling *et al.* (2010)). We define $f(\theta)$ as the steady direction distribution given by

$$f = \frac{1}{\int_{-\pi}^{\pi}\frac{1}{\lambda(\theta)}d\theta}\frac{1}{\lambda}. \tag{2.36}$$

This distribution satisfies the equation

$$\lambda f - \int_{-\pi}^{\pi}\lambda(\theta')K(\theta,\theta')f(\theta')d\theta' = 0, \tag{2.37}$$

subject to the constraint $\int_{-\pi}^{\pi}f(\theta)d\theta = 1$. This represents an equilibrium distribution for which cells are turning away from angle θ at the same rate they are turning towards the angle θ.

We define the mean component of cell direction up the gradient as

$$\overline{p_y} = \int_{-\pi}^{\pi}\sin\theta f(\theta)d\theta. \tag{2.38}$$

The mean drift, $V_s\overline{p_y}$, non-dimensionalised on the characteristic speed $L/T = \varepsilon V_s$ is given by $\frac{1}{\varepsilon}\overline{p_y}$. Recall here that L is defined as the characteristic length scale and T the characteristic time scale for diffusion to act over the length scale L: $T = L^2\lambda_0/V_s^2 = 1/(\varepsilon^2\lambda_0)$. We therefore consider a change of reference frame moving with the mean drift:

$$y = z + \frac{1}{\varepsilon}\overline{p_y}t, \tag{2.39}$$

and transform equation (2.14):

$$\varepsilon^2\frac{\partial\psi}{\partial t} + \varepsilon\frac{\partial}{\partial z}((\sin\theta - \overline{p_y})\psi) + \lambda\psi - \int_{-\pi}^{\pi}\lambda(\theta')K(\theta,\theta')\psi(\theta')d\theta' = 0. \tag{2.40}$$

Integrating this equation over θ gives the conservation equation

$$\varepsilon^2\frac{\partial n}{\partial t} + \varepsilon\frac{\partial}{\partial z}\int_{-\pi}^{\pi}(\sin\theta - \overline{p_y})\psi d\theta = 0. \tag{2.41}$$

We now make use of the fact that $\varepsilon \ll 1$ and consider a perturbation expansion for ψ:

$$\psi = \psi^{(0)}(z,\theta,t) + \varepsilon\psi^{(1)}(z,\theta,t) + \cdots. \tag{2.42}$$

Equation (2.40) yields at leading order

$$\lambda\psi^{(0)} = \int_{-\pi}^{\pi}\lambda(\theta')K(\theta,\theta')\psi^{(0)}(\theta')d\theta'. \tag{2.43}$$

As shown in appendix A, for the turn kernels we are considering, equation (2.12), the leading order solution is given by

$$\psi^{(0)}(z,\theta,t) = f(\theta)n^{(0)}(z,t). \tag{2.44}$$

In contrast to the perturbation expansion for weak chemotactic response, equation (2.25), we see that now at leading order the cells are not isotropically distributed because the chemotactic bias is a leading order effect.

Equation (2.40) yields

At $O(\varepsilon)$:

$$(\sin\theta - \overline{p_y})f\frac{\partial n^{(0)}}{\partial z} + \lambda\psi^{(1)} - \int_{-\pi}^{\pi}\lambda(\theta')K(\theta,\theta')\psi^{(1)}(\theta')d\theta' = 0. \tag{2.45}$$

As shown in appendix A, the solution to this equation is given by

$$\psi^{(1)} = -f^{(1)}(\theta)\frac{\partial n^{(0)}}{\partial z} + f(\theta)n^{(1)} \tag{2.46}$$

where $f^{(1)}(\theta)$ satisfies

$$\lambda f^{(1)} - \int_{-\pi}^{\pi}\lambda(\theta')K(\theta,\theta')f^{(1)}(\theta')d\theta' = (\sin\theta - \overline{p_y})f, \tag{2.47}$$

$$\int_{-\pi}^{\pi}f^{(1)}(\theta)d\theta = 0. \tag{2.48}$$

We can now compute

$$\int_{-\pi}^{\pi}(\sin\theta-\overline{p_y})\psi^{(1)}d\theta=-\frac{\partial n^{(0)}}{\partial z}\int_{-\pi}^{\pi}(\sin\theta-\overline{p_y})f^{(1)}d\theta, \tag{2.49}$$

and thus the conservation equation (2.41) yields the diffusion equation at leading order:

$$\frac{\partial n^{(0)}}{\partial t}-\frac{\partial}{\partial z}\left(D\frac{\partial n^{(0)}}{\partial z}\right)=0, \tag{2.50}$$

where

$$D=\int_{-\pi}^{\pi}(\sin\theta-\overline{p_y})f^{(1)}d\theta. \tag{2.51}$$

Reverting to fixed-frame non-dimensional variables gives the drift-diffusion equation

$$\frac{\partial n^{(0)}}{\partial t}+\frac{\partial}{\partial y}\left(\frac{1}{\varepsilon}\overline{p_y}n^{(0)}-D\frac{\partial n^{(0)}}{\partial y}\right)=0. \tag{2.52}$$

As for weak chemotaxis, to examine the explicit dependence of chemotactic drift and diffusion on speed and turn rate, it is helpful to write this equation in terms of dimensional quantities:

$$\frac{\partial n^{(0)}}{\partial t^*}+\frac{\partial}{\partial y^*}\left(V_s\overline{p_y}n^{(0)}-\frac{V_s^2}{\lambda_0}D\frac{\partial n^{(0)}}{\partial y^*}\right)=0. \tag{2.53}$$

2.5 *Individual based simulations*

To test out the predictions of the theory, we compare with the results of individual-based stochastic simulations for isotropic tumbles. In the individual based simulations, we choose to non-dimensionalise time on λ_0, and so define a new non-dimensional time, $\tau=\lambda_0 t^*$, which is related to t by $t=\varepsilon^2\tau$. We initialise N bacteria at $y=y_0$ and draw the initial cell direction, $\theta_i(0)$ of the ith bacterium from the standard uniform distribution on the open interval $(-\pi,\pi)$. At each time interval $\Delta\tau$, with probability $\lambda(\theta_i)\Delta\tau\ll 1$, the bacteria tumbles and its direction is updated to a new value of θ drawn from the standard uniform distribution on the open interval $(-\pi,\pi)$. In each time interval $\Delta\tau$, the position y_i is updated because the bacterium moves a distance $\varepsilon\Delta\tau\sin\theta_i$. We impose reflective boundary conditions at $y=0$ and $y=1$ such that if the updated position of bacterium at time $\tau+\Delta\tau$ given by $y_i(t)+\varepsilon\Delta\tau\sin\theta_i<0$ with direction θ_i such that $\sin\theta_i<0$ then we reflect so that the position of bacterium at time $\tau+\Delta\tau$ given by $y_i(t)-\varepsilon\Delta\tau\sin\theta_i>0$ with direction $-\theta_i$. A similar condition is imposed at $y=1$. The numerical simulations were implemented in Matlab2016a using the inbuilt random number generator *rand*, with default parameters $y_0=0.2,\Delta\tau=0.1$. We verified convergence by repeating the simulations using $\Delta\tau=0.05$.

3. Results

3.1 *Weak chemotaxis model is insufficient to examine difference between optimistic and pessimistic strategies*

Consider an optimistic strategy with weak chemotaxis, taking a linear approximation of equation (2.17) as the tumble rate:

$$\lambda=1-\varepsilon\chi\sin\theta H(\sin\theta). \tag{3.1}$$

For mathematical simplicity, we focus attention on isotropic tumbles, taking

$$K(\theta,\theta') = \frac{1}{2\pi}. \tag{3.2}$$

With this form for the tumble rate, the leading order first moment equation (2.31) becomes

$$\frac{\partial Q^{(0)}}{\partial y} + j^{(1)} - \chi Q^{(0)+} = 0, \tag{3.3}$$

where $Q^{(0)+} = \int_0^\pi \sin^2\theta \psi^{(0)} d\theta$. On taking $\psi^{(0)} = \frac{1}{2\pi} n^{(0)}$, we obtain the drift-diffusion chemotaxis equation found previously, but with the drift term being halved:

$$\frac{\partial n^{(0)}}{\partial t} + \frac{1}{2}\frac{\partial}{\partial y}\left(\frac{1}{2}\chi n^{(0)} - \frac{\partial n^{(0)}}{\partial y}\right) = 0. \tag{3.4}$$

The exact same chemotactic drift-diffusion equation is found for the pessimistic strategy for which the tumble rate is increased if moving down a chemical gradient, but unchanged if moving up the gradient:

$$\lambda = 1 - \varepsilon\chi \sin\theta H(-\sin\theta). \tag{3.5}$$

Although the average run duration for pessimists with tumble rate given by equation (3.5) is longer than the average run duration for optimists, this does not affect the diffusion because modifying the tumble rate only changes the drift component, not the diffusive component.

3.2 *Results for strong chemotaxis, isotropic tumbles*

We now obtain explicit expressions for the drift and diffusion coefficients for strong chemotaxis, assuming isotropic tumbles, $K(\theta,\theta') = 1/2\pi$. We initially obtain results for the bi-biased cells, and then compare the optimistic and pessimistic strategies.

3.2.1 *Calculation of drift & diffusion coefficients* From equations (2.38,2.51), the mean component of cell direction up the gradient and non-dimensional diffusion coefficient are defined as functions of the equilibrium direction distribution f, given by equation (2.36) (depicted in Fig. 1(a)), and $f^{(1)}$ which satisfies equation (2.47) with $K(\theta,\theta') = 1/2\pi$:

$$\lambda f^{(1)} - \frac{1}{2\pi}\int_{-\pi}^{\pi} \lambda(\theta') f^{(1)}(\theta') d\theta' \quad = \quad (\sin\theta - \overline{p_y}) f. \tag{3.6}$$

On rearranging this equation, the function $f^{(1)}$ can be written as

$$f^{(1)}(\theta) = \frac{C_1 + (\sin\theta - \overline{p_y}) f(\theta)}{\lambda(\theta)}, \tag{3.7}$$

where the unknown constant $C_1 = \frac{1}{2\pi}\int_{-\pi}^{\pi} \lambda(\theta') f^{(1)}(\theta') d\theta'$. The constant C_1 is determined on applying the normalisation condition $\int_{-\pi}^{\pi} f^{(1)} d\theta = 0$ introduced in equation (2.48):

$$\int \frac{C_1 + (\sin\theta - \overline{p_y}) f(\theta)}{\lambda(\theta)} d\theta = 0 \tag{3.8}$$

$$\Rightarrow C_1 = -\int \frac{(\sin\theta - \overline{p_y}) f(\theta)}{\lambda(\theta)} d\theta \Big/ \int \frac{1}{\lambda(\theta)} d\theta \,. \tag{3.9}$$

Furthermore on inserting equation (3.7) into equation (2.51), and making use of equations (2.36,2.38), we obtain the following expression for the diffusion coefficient solely in terms of the equilibrium direction distribution:

$$D = \int_{-\pi}^{\pi} \frac{f(\theta)}{\lambda(\theta)} (\sin\theta - \overline{p_y})^2 d\theta. \tag{3.10}$$

This integral was computed numerically using Matlab2016a for bi-bias, optimist and pessimist strategies as given by tumble rates specified by equations (2.15,2.17,2.18), for a range of chemotactic strengths, χ.

In Fig. 1(b), for small values of $\varepsilon\chi$ we see agreement with the weak chemotactic calculations, $\overline{p_y} \sim \frac{1}{2}\varepsilon\chi$ for bi-bias, and $\overline{p_y} \sim \frac{1}{4}\varepsilon\chi$ for optimists and pessimists. The drift is less for optimists and pessimists than bi-bias because cells only respond to the gradient when moving down (pessimist) or up (optimist) the gradient. As the chemotactic strength increases, the value of $\overline{p_y}$ saturates. For optimist and bi-bias cells the mean direction tends toward movement that is purely up the gradient, $\overline{p_y} = 1$. However, pessimist cells are equally likely to move in any direction with a positive component up the gradient, so $\overline{p_y} \to \frac{1}{\pi}\int_0^{\pi} \sin\theta d\theta = 2/\pi$ as $\varepsilon\chi \to \infty$.

In Fig. 1(b), we see the effect of bias on the diffusion rate which contrasts with the weak chemotaxis calculations where diffusion was unaffected by chemotactic bias. We see that pessimistic cells have a lower diffusion rate than bi-bias cells which in turn have a lower diffusion rate than optimistic cells. This can be explained because of the relative average run duration; pessimistic cells have the shortest average run duration because the run duration is reduced when moving down the gradient whereas optimistic cells have the longest average run duration because the run duration is increased when moving up the gradient. Furthermore, whereas pessimistic cells have a monotonic decrease in diffusion rate with chemotactic strength, bi-bias and optimistic cells display a more complex relationship with chemotactic strength.

3.2.2 *Computing spatial aggregation* We now consider the spatial distribution of cell concentration, $n^{(0)}(y,t)$ for a bounded region, where there is zero cell flux at boundaries $y = 0$ and $y = 1$. The equilibrium, no-flux, solution to the drift-diffusion equation (2.52) with unit mass is given by

$$n^{(0)} = \frac{\mu}{e^{\mu} - 1} e^{\mu y}, \quad \text{where} \quad \mu = \frac{\overline{p_y}}{\varepsilon D}. \tag{3.11}$$

We can interpret $1/\varepsilon = L\lambda_0/V_s$ as the height of the chamber non-dimensionalised on V_s/λ_0, and thus we can see how the equilibrium distribution will vary with the height of the chamber.

In Fig. 1(d) we see that the ratio of drift to diffusion, which determines the equilibrium distribution, is always greater for bi-bias and pessimists than for optimists, and when $\varepsilon\chi \gtrsim 2$ the ratio is greatest for the pessimist strategy. This indicates that pessimists are better able to concentrate in preferred regions when the chemotactic strength is sufficiently high; as indicated in the final distribution of cells depicted in Fig. 2(f).

Furthermore, in Fig. 1(e) we identify how cell speed, non-dimensionalised on $L\lambda_0$, given by parameter $\varepsilon = V_s/L\lambda_0$, affects μ, the exponent of the steady state accumulation. For the weak chemotaxis model, with $\overline{p_y} \propto \varepsilon\chi$, and D a constant, steady state accumulation is independent of ε, as previously observed (e.g. Son *et al.*, 2016). In contrast, for strong chemotaxis the steady-state accumulation varies with cell speed and strategy. For optimists, the accumulation decreases monotonically with cell speed, whereas for bi-bias and pessimists there is an initial increase, followed by decrease. In particular, for

pessimists, faster speeds result in a two-fold increase in μ, from $\mu = \chi/2$ when $\varepsilon = 0$ to a maximum of $\mu = \chi$. The non-intuitive prediction of non-uniform accumulation at zero swimming speed, $\varepsilon = 0$, arises from $\mu = \frac{\overline{p_y}}{\varepsilon D} \to \chi/2$ in the limit of $\varepsilon \to 0$. However, this non-uniform accumulation would take an infinite time to be realised as, when non-dimensionalised on L and λ_0, the drift, $\varepsilon\overline{p_y}$, and diffusion, $\varepsilon^2 D$, both tend to zero as $\varepsilon \to 0$.

To examine the transient distribution we numerically solved the drift-diffusion equation (2.52) for a region $y \in (0,1)$ with reflective boundary conditions (Fig. 2) taking a sharply peaked unit mass Gaussian centred around $y_0 = 0.2$. Solutions were obtained using the Matlab2016a *pdepe* solver, taking $\varepsilon = 0.1$. The solution obtained at $t = 1$ is indistinguishable from the equilibrium solution, equation (3.11). We note that because pessimists have a lower diffusion rate they take longer to attain the equilibrium distribution.

3.3 *Investigating the impact of non-isotropic tumbles for strong chemotaxis*

We shall now consider two examples of non-isotropic tumbles. Firstly we shall consider a standard model of persistence, whereby the new direction post-tumble is positively correlated with the pre-tumble direction. We shall then consider modelling the run-reverse strategy where cells approximately reverse direction between runs. We assume the turn kernel satisfies the Von-Mises distribution:

$$K(\theta,\theta') = h(|\theta-\theta'|) = \frac{1}{2\pi I_0(\kappa)} \exp\left(\kappa\cos(\theta-\theta')\right), \tag{3.12}$$

where I_0 is the modified Bessel function of order 1. Note that κ is related to the index of persistence, α:

$$\alpha = 2\int_0^\pi \cos u h(u) du = \frac{I_1(\kappa)}{I_0(\kappa)}. \tag{3.13}$$

Experiments have shown that the movement of *E. coli* closely matches this turn kernel for $\alpha = 0.46$ (Taylor-King *et al.*, 2015). When $\kappa > 0$, the turn kernel represents persistence, whereby the distribution of new directions, θ, is peaked around the pre-tumble direction, θ'.

For a pure run-reverse movement, the turn kernel is given by

$$K(\boldsymbol{p},\boldsymbol{p}') = \delta(\boldsymbol{p}+\boldsymbol{p}'), \tag{3.14}$$

where δ is the Dirac delta function, equal to zero except when $\boldsymbol{p} = -\boldsymbol{p}'$. The index of persistence for this strategy is $\alpha = -1$. In order to generate a random walk which is not restricted to purely the initial direction $\boldsymbol{p}_0$ and the reverse direction $-\boldsymbol{p}_0$ we could include rotational diffusion in the model. Alternatively, we can approximate a run-reverse strategy by taking a sufficiently large negative value of $\kappa < 0$ in the Von-Mises turn kernel. For example, a value of $\kappa = -10$ yields a persistence index of $\alpha = -0.9486$.

The governing drift-diffusion equation (2.52), with coefficients defined by eq. (2.38, 2.51) is still valid. The steady direction distribution, f, and hence the drift coefficient are unchanged for non-isotropic tumbles. However the function $f^{(1)}$ which appears in the diffusion coefficient and is defined in eq. (2.47) has now to be computed numerically as the solution of a Fredholm equation of the second type (see appendix C for details).

The effect of persistence on the diffusion rate for the different strategies is depicted in Fig. 3. For $\varepsilon\chi = 0$ we have that $D = (1-\alpha)/2$, in agreement with equation (2.32) found for weak chemotaxis. As

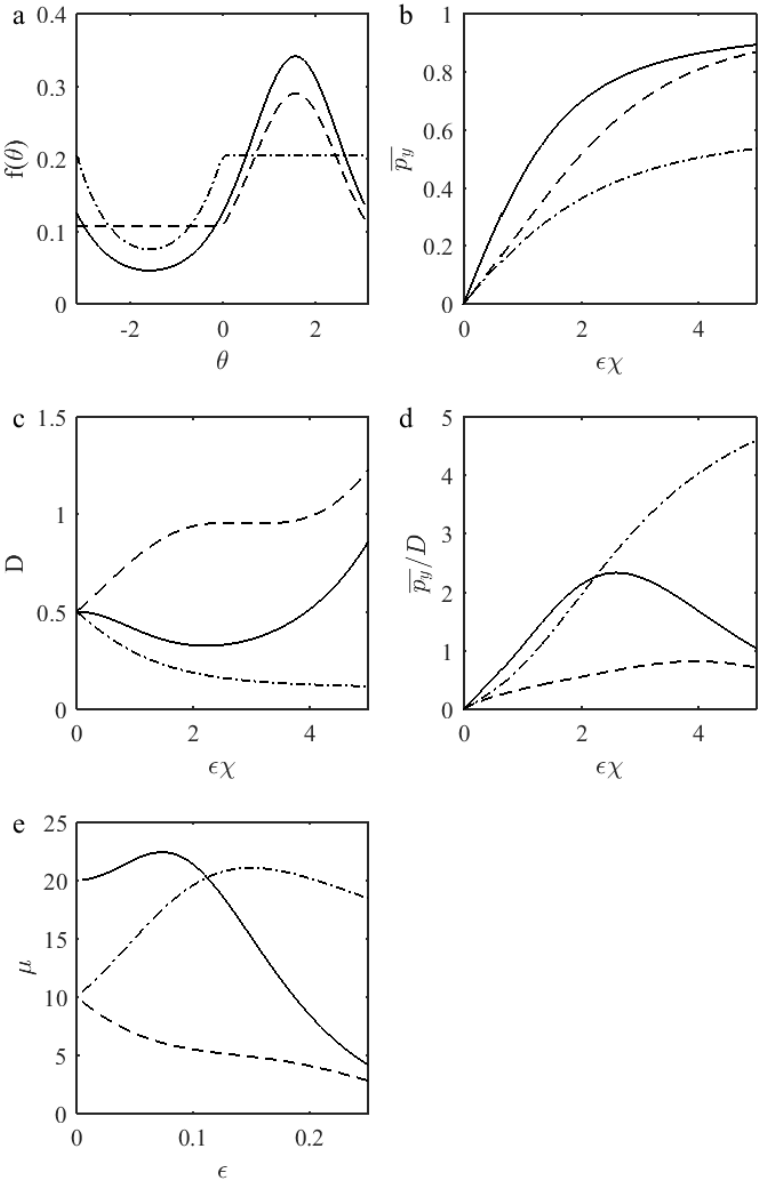

FIG. 1. Drift & diffusion coefficients for bi-bias (Solid line); optimist (Dashed line); pessimist (Dash-dot). (a) Equilibrium direction distribution, $f(\theta)$, for chemotactic strength $\varepsilon\chi = 1$; (b) Mean component of cell direction up the gradient, $\overline{p_y}$, as a function of $\varepsilon\chi$; (c) Non-dimensional diffusion constant, D, as a function of $\varepsilon\chi$; (d) Ratio of $\overline{p_y}$ to D as a function of $\varepsilon\chi$; (e) Equilibrium exponent, $\mu = \frac{\overline{p_y}}{\varepsilon D}$ as a function of $\varepsilon = V_s/L\lambda_0$, the cell speed non-dimensionalised on $L\lambda_0$, for $\chi = 20$.

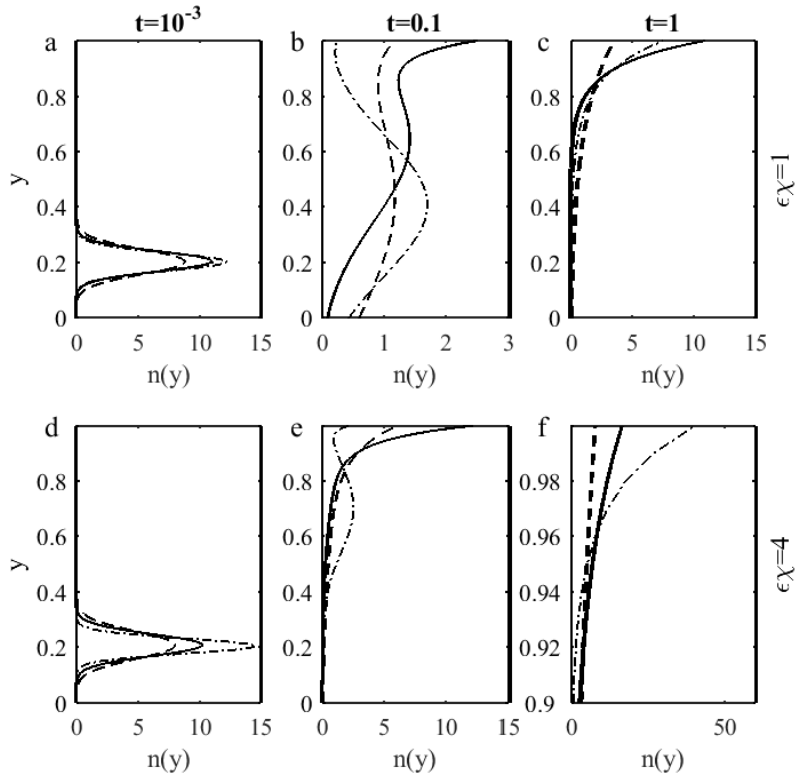

FIG. 2. Solution to drift-diffusion equation with no flux boundary conditions for bi-bias (Solid line); optimistic (Dashed line); pessimistic (Dash-dot) strategies at times $t = 10^{-3}$ (a,d), $t = 0.1$ (b,e), $t = 1$ (c,f) for chemotactic strength $\varepsilon\chi = 1$ (a,b,c) and $\varepsilon\chi = 4$ (d,e,f).

for the case of weak chemotaxis, an increase in the index of persistence results in an increase in diffusion rate for all strategies. An increase in persistence will result in cells being able to search their environment more rapidly, but they will be less able to concentrate in preferred regions. In contrast, when the index of persistence is negative, representative for example of the run-reverse strategy, cells will search their environment more slowly, but they will be better able to concentrate in preferred regions. The effect of persistence on the diffusion rate becomes less pronounced as the chemotactic strength increases, but it appears that the run-reverse and isotropic turn kernel converge to a diffusion rate slightly lower than the turn kernel with positive persistence for all three chemotactic strategies (bi-bias, optimistic and pessimistic).

3.4 *Orthotaxis*

Many chemicals affect the speed at which cells move. These changes in cell speed can be classified into two categories: chemokinesis occurs when cell speed depends on the local concentration of a chemical, whereas orthotaxis occurs when cell speed depends on the local chemical gradient. Motivated by recent experiments, which found that biofilm cells move faster up chemoattractant gradients than down them (Oliveira *et al.*, 2016), here we investigate the effect of orthotaxis by allowing the cell speed to depend on its direction of movement. Equation (2.14) becomes

$$\varepsilon^2\frac{\partial\psi}{\partial t} + \varepsilon\frac{\partial}{\partial y}(v(\theta)\sin\theta\psi) + \lambda\psi - \int_{-\pi}^{\pi}\lambda(\theta')K(\theta,\theta')\psi(\theta')d\theta' = 0, \tag{3.15}$$

where the function $v(\theta)$ describes how the non-dimensional speed varies as function of direction, θ.

We consider the case where the tumble rate is uniform, $\lambda = 1$, tumbles are isotropic, $K(\theta,\theta') = \frac{1}{2\pi}$, and there is only a weak bias in cell speed corresponding to faster movement up the gradient:

$$v(\theta) = 1 + \varepsilon\nu\sin\theta, \tag{3.16}$$

where ν is defined as the coefficient of orthotaxis. Equation (3.15) reduces to

$$\varepsilon^2\frac{\partial\psi}{\partial t} + \varepsilon\frac{\partial}{\partial y}((1+\varepsilon\nu\sin\theta)\sin\theta\psi) + \psi - \frac{1}{2\pi}n = 0. \tag{3.17}$$

Taking moments of equation (3.17) yields:

$$\varepsilon^2\frac{\partial n}{\partial t} + \varepsilon\frac{\partial j}{\partial y} + \varepsilon^2\nu\frac{\partial Q}{\partial y} = 0, \tag{3.18}$$

$$\varepsilon^2\frac{\partial j}{\partial t} + \varepsilon\frac{\partial Q}{\partial y} + \varepsilon^2\nu\frac{\partial P}{\partial y} + j = 0, \tag{3.19}$$

where we have introduced the third order moment $P = \int_{-\pi}^{\pi}\sin^3\theta\psi d\theta$. As previously, we consider a perturbation expansion for ψ:

$$\psi = \frac{1}{2\pi}n^{(0)}(y,t) + \varepsilon\psi^{(1)}(y,\theta,t) + \cdots, \tag{3.20}$$

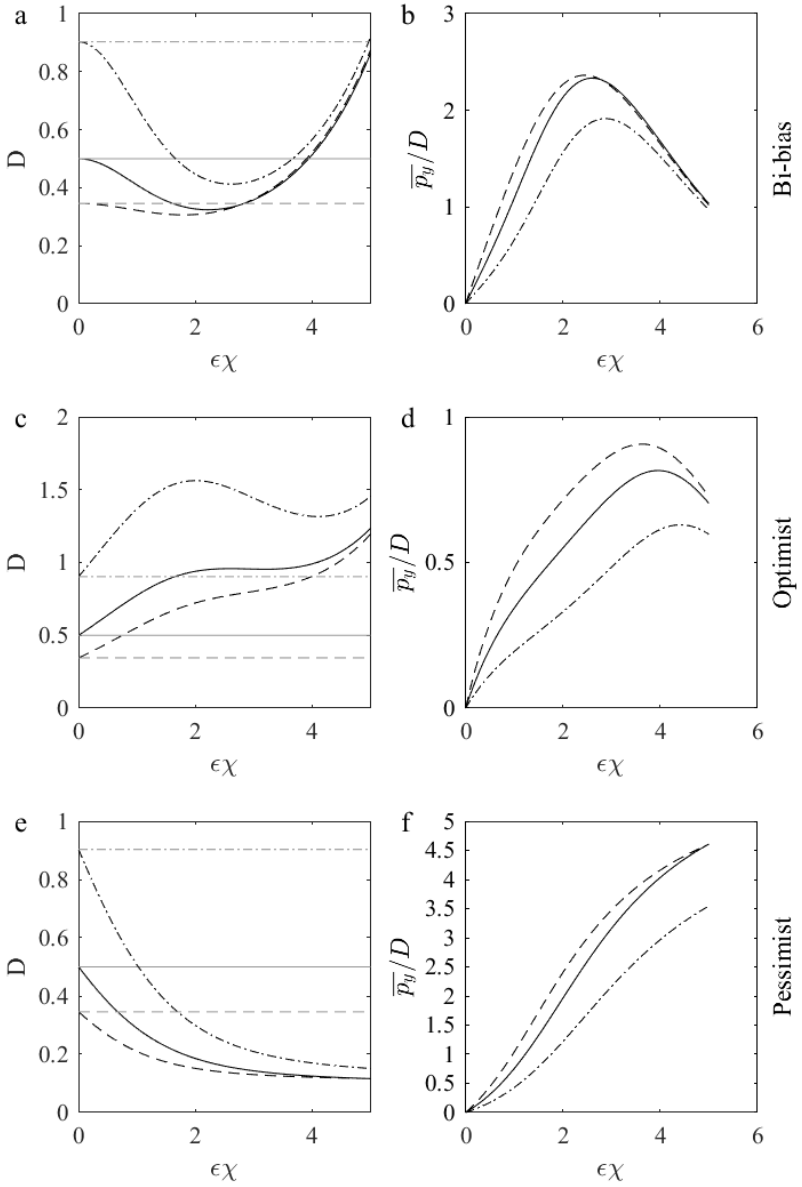

FIG. 3. Investigating effect of persistence on diffusion coefficient and chemotactic clustering: isotropic tumbles (Solid line); negative persistence $\kappa = -1$ (Dashed line); positive persistence $\kappa = 1$ (Dash-dot). Left-hand panels are non-dimensional diffusion constant, D, as a function of $\varepsilon\chi$ and right-hand panels are ratio of $\overline{p_y}$ to D as a function of $\varepsilon\chi$. (a,b) Bi-bias; (c,d) Optimist; (e,f) Pessimist. Horizontal lines indicate diffusion coefficient for weak chemotaxis, $D = 1/2(1-\alpha)$ where α is index of persistence.

which yields $j^{(0)} = P^{(0)} = 0$ and $Q^{(0)} = \frac{1}{2}n^{(0)}(y,t)$. At leading order in ε, equations (3.18) and (3.19) thus give

$$\frac{\partial n^{(0)}}{\partial t} + \frac{\partial j^{(1)}}{\partial y} + \nu \frac{\partial Q^{(0)}}{\partial y} = 0, \tag{3.21}$$

$$\frac{\partial Q^{(0)}}{\partial y} + j^{(1)} = 0, \tag{3.22}$$

which, on inserting the expression $Q^{(0)} = \frac{1}{2}n^{(0)}(y,t)$, can be rearranged to give a single equation for $n^{(0)}$:

$$\frac{\partial n^{(0)}}{\partial t} + \frac{1}{2}\frac{\partial}{\partial y}\left(\nu n^{(0)} - \frac{\partial n^{(0)}}{\partial y}\right) = 0, \tag{3.23}$$

which in dimensional variables is given by

$$\frac{\partial n^{(0)}}{\partial t^*} + \frac{\partial}{\partial y^*}\left(\frac{1}{2}\varepsilon \nu V_s n^{(0)} - \frac{V_s^2}{2\lambda_0}\frac{\partial n^{(0)}}{\partial y^*}\right) = 0. \tag{3.24}$$

We can relate the ratio of cell speed up and down the gradient to the drift velocity. We have that

$$\frac{v_{down}}{v_{up}} \approx 1 - 2\varepsilon\nu \tag{3.25}$$

and so the mean movement along the gradient is given by

$$\frac{1}{2}\varepsilon\nu V_s \approx \frac{1}{4}(1 - \frac{v_{down}}{v_{up}})V_s. \tag{3.26}$$

3.5 *Comparison with experiments*

Oliveira *et al.* (2016) show that surface attached *P. aeruginosa* cells use a pessimistic strategy and their reversal rate nearly doubles when they move down a chemoattractant gradient. Comparing the tumble rate for $\theta = \pi/2$ (up gradient) with the tumble rate at $\theta = -\pi/2$ (down gradient) in our model of strong chemotaxis, equation (2.18), allows us to estimate the chemotactic strength as $\varepsilon\chi = \ln 2$. Using the expressions in section 3.2.1 and assuming isotropic tumbles, we then can predict the mean component of cell motility directed along the gradient is $\overline{p_y} = 0.16$ and the non-dimensional diffusion coefficient is $D = 0.34$. In contrast, to obtain the same bias the weak chemotaxis model (section 3.1) requires that $\varepsilon\chi = 1$. While this clearly violates the underlying assumption of the weak chemotaxis model that $\varepsilon\chi \ll 1$, for $\varepsilon\chi = 1$ the weak chemotaxis model predicts that the mean fraction of motility directed along the gradient is $\frac{1}{4}\varepsilon\chi = 1/4$ and the diffusion coefficient is $D = 1/2$, the latter of which is independent of the bias. Therefore, in this limit the weak chemotaxis model overestimates both the drift and diffusion by approximately 50%. Of course, cells within biofilms do not perform isotropic tumbles, but instead exhibit run-reverse movement that can modelled using a negative persistence. Our results for the strong chemotaxis model show that the chemotactic drift is independent of the value of persistence, but diffusion is reduced for cells that exhibit run-reverse behaviour (Fig. 3).

Aside from a bias in the reversal rate, another way for a population of cells to generate a net drift along a chemical gradient is via the modulation of cell speed. Oliveira *et al.* (2016) find that *P. aeruginosa* move 25% faster when moving up a gradient than when moving down a gradient, suggesting that this orthotactic response may help facilitate a population's movement along gradients. Using the weak orthotactic approximation given by equation (3.26) these values yield a mean drift of 5% of the cell speed and thus within the modelling framework presented here, orthotaxis appears less important than bias in reversal rate. However, this calculation is only a rough approximation and assumes that they do not preferentially bias their runs up chemoattractant gradients. Further studies will be required to ascertain how variation in cell speed interacts with a strong chemotactic response.

3.6 *Comparison with individual-based simulation*

In Fig. 4(a-c) the spatial distribution of cells from an individual-based simulation, described in section 2.5, is compared with the numerical solution of the drift-diffusion equation (2.52) with zero cell flux at boundaries $y = 0$ and $y = 1$, for chemotactic strength $\varepsilon\chi = 1$, and $\varepsilon = 0.1$. These results are for a bi-bias strong chemotactic response with isotropic tumbles, and so the drift and diffusion coefficients are as calculated in section (3.2.1) with non-linear tumble rate defined by equation (2.15). As expected, on time-scales long compared to that of individual steps in the random walk, we see good agreement in the spatial distribution. Specifically, $t = 0.1$ corresponds to a time of $\tau = t/\varepsilon^2 = 10$ non-dimensionalised on runs of typical duration $1/\lambda_0$.

Further evidence for the agreement between the individual-based simulation and numerical solution of the drift-diffusion equation is provided in Fig. 5, where a larger domain, given by $\varepsilon = 0.01$, and larger chemotactic strength $\varepsilon\chi = 2$, is investigated. We show how the spatial distribution is affected by the chemotactic strategy, that is whether cells use a bi-bias, optimistic, or pessimistic strategy as defined through their tumble rate functions, equations (2.15, 2.17, 2.18). In all cases we assume isotropic tumbles. We see that the velocity of the peak in the distribution is largest for the bi-bias strategy and smallest for the pessimistic strategy. Moreover, the optimistic strategy generates cells distribution that are less peaked than the other two strategies. These results are consistent with our calculations of the drift and diffusion coefficients shown in Fig. 1.

We also see in Fig. 4(f,g) that the direction distribution agrees well for intermediate times. However, we note that as the equilibrium spatial distribution is attained, the direction distribution appears approximately uniform (Fig. 4(h)) in contrast to the direction distribution predicted by equation (2.36).

In Fig. 6(a-c) we see that there is agreement between the equilibrium predictions from the drift-diffusion model and the individual-based simulations when examining optimistic and pessimistic strategies. Here we examine how the equilibrium spatial distribution is affected by the chemotactic strength, as measured by $\varepsilon\chi$, and the chemotactic strategy, that is whether cells are bi-bias, optimistic, or pessimistic. Specifically, these simulations validate our finding that the pessimistic strategy is better than the optimistic strategy at concentrating in preferred regions for all chemotactic strengths considered. However, as the chemotactic strength is increased, we note a discrepancy in predictions; with the drift-diffusion model under-predicting the aggregation for pessimists and bi-bias strategies, and over-predicting the aggregation of optimists.

To understand this discrepancy, we return to the full governing equation for ψ, equation (2.14) and

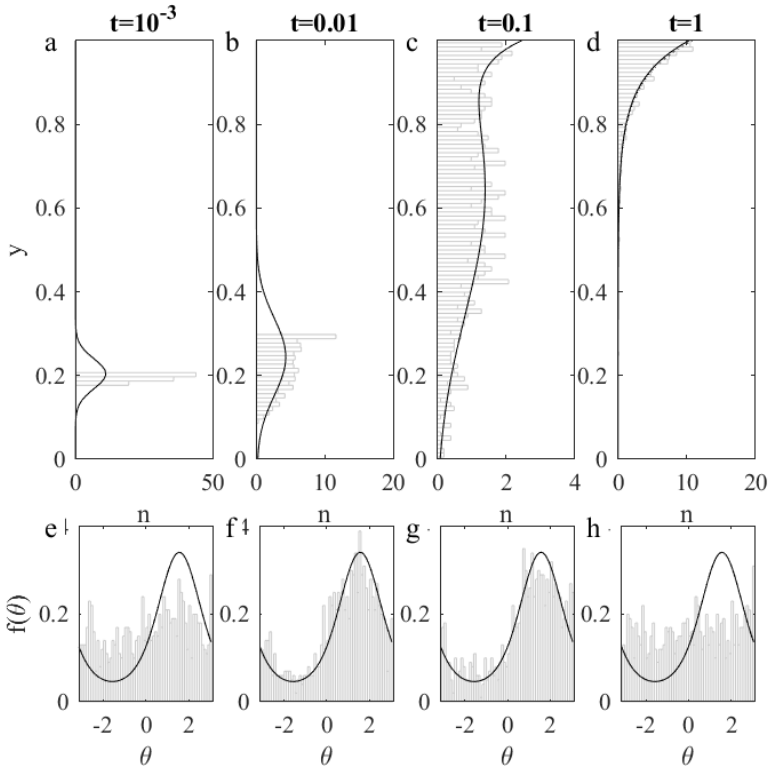

FIG. 4. Comparison of individual-based stochastic simulations with solution to drift-diffusion equation for bi-bias at times (a) $t = 10^{-3}$, (b) $t = 0.01$, (c) $t = 0.1$, and (d) $t = 1$ for chemotactic strength $\varepsilon\chi = 1$, and $\varepsilon = 0.1$. Histogram is result from individual based simulations, with $\Delta\tau = 0.1$, solid line is solution of drift-diffusion equation as Fig. 2. The corresponding direction distribution at the same times are given in (e-g); histogram is result from individual based simulation, solid line is direction distribution given by equation (2.36).

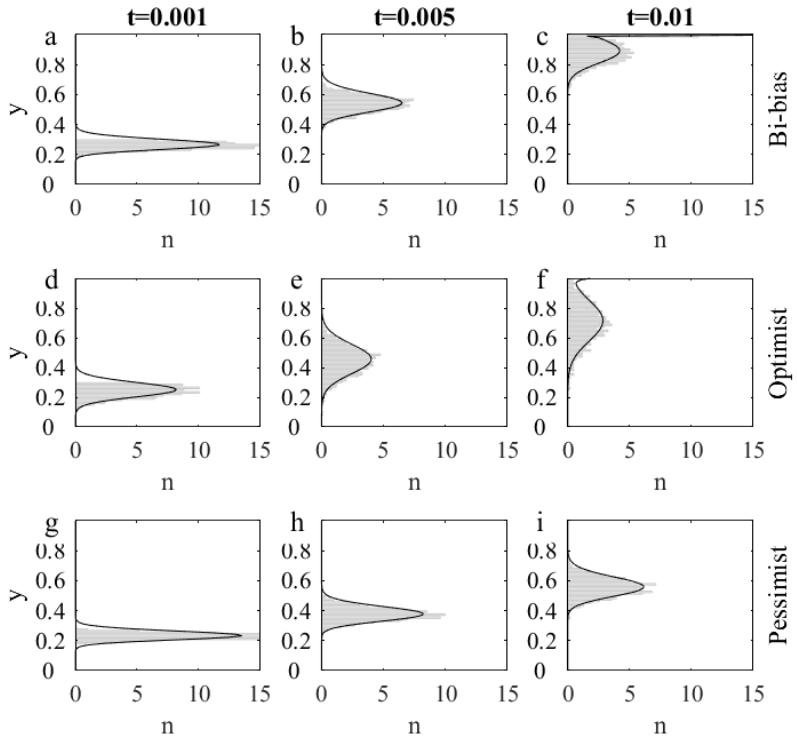

FIG. 5. Comparison of individual-based stochastic simulations with solution to drift-diffusion equation for a larger domain represented by $\varepsilon = 0.01$, with chemotactic strength $\varepsilon\chi = 2$. Histogram is result from individual based simulations, with $\Delta\tau = 0.01$, solid line is solution of drift-diffusion equation with no flux boundary conditions.

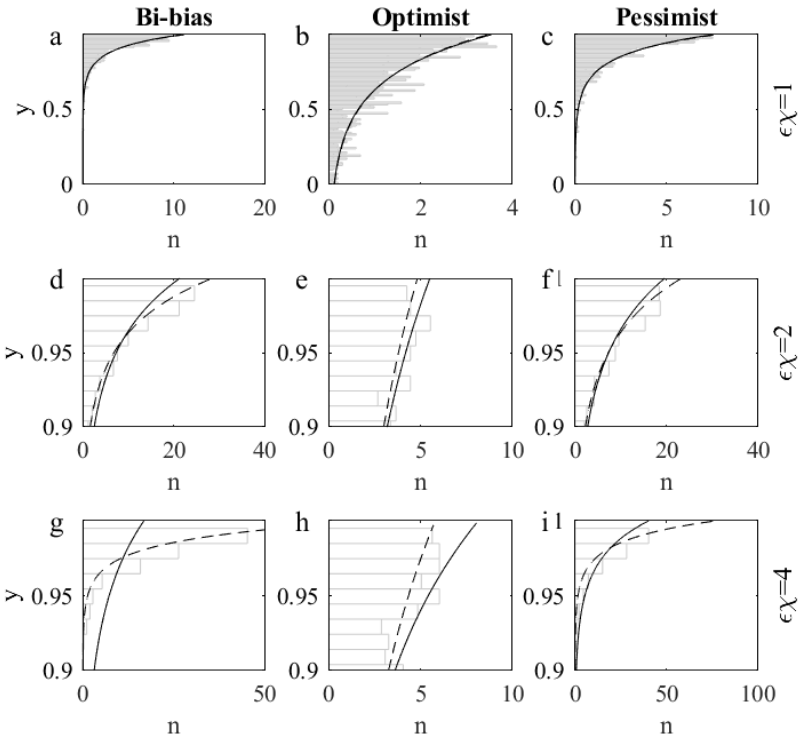

FIG. 6. Comparison of equilibrium spatial distribution in individual-based stochastic simulations (histogram) with equilibrium solution to drift-diffusion equation (solid line) and direct equilibrium solution (dashed line) for (a,d,g) bi-bias; (b,e,h) optimist; (c,f,i) pessimist. Chemotactic strength: (a,b,c) $\varepsilon\chi = 1$; (d,e,f) $\varepsilon\chi = 2$; (g,h,i) $\varepsilon\chi = 4$.

consider the equilibrium solution with isotropic tumbles:

$$\varepsilon \frac{\partial}{\partial y}(\sin\theta\psi) + \lambda\psi - \frac{1}{2\pi}\int_{-\pi}^{\pi}\lambda(\theta')\psi(\theta')d\theta' = 0. \tag{3.27}$$

At the boundary, we impose zero cell flux. To interpret this as a boundary condition on ψ, as in Bearon & Hazel (2015), we note that the integral of equation (2.14) over θ yields the conservation equation (2.23) for cell density

$$\varepsilon \frac{\partial n}{\partial t} + \frac{\partial j}{\partial y} = 0, \tag{3.28}$$

where $j = \int_{-\pi}^{\pi}\sin\theta\psi d\theta$ is the vertical flux of cells. At equilibrium, j must be independent of y and therefore is zero everywhere:

$$\int_{-\pi}^{\pi}\sin\theta\psi d\theta = 0. \tag{3.29}$$

By inspection, we can propose a solution to equation (3.27) subject to boundary condition (3.29):

$$\psi = \frac{1}{\beta\sin\theta + \lambda}\exp\left(\frac{\beta y}{\varepsilon}\right), \tag{3.30}$$

where β is defined by the no-flux condition, $\int_{-\pi}^{\pi}\sin\theta\psi d\theta = 0$:

$$\int_{-\pi}^{\pi}\frac{\sin\theta}{\beta\sin\theta + \lambda}d\theta = 0. \tag{3.31}$$

This direct equilibrium solution for cell concentration agrees well with results from the individual-based simulation as shown in Fig. 6, and the direct equilibrium direction distribution also agrees well with results from the individual based simulations as shown in Fig. 7. However, whilst we have been able to obtain a more accurate prediction for the equilibrium distribution, further work is needed to derive the corresponding governing equation to describe the temporal evolution of the cell concentration, and to determine whether this can be described by a drift-diffusion equation.

4. Discussion

This work develops a mathematical framework to predict how populations of bacteria move and distribute within chemical gradients. The framework assumes cells move along a two-dimensional surface where cells move along straight 'runs' that are interspersed by reorientation events. We have explicitly identified the relationship between the population-level chemotactic drift and diffusion, and the reorientation rate and turn kernel for when the bias in reorientation rate strongly depends on the chemoattractant gradient. We have also investigated how the drift-diffusion approximation obtained through a singular perturbation analysis compares with individual-based stochastic simulations. When comparing our drift-diffusion approximation to individual-based simulations, we observed a breakdown of the drift-diffusion continuum models due to the presence of the no-flux boundary, as previously observed in the context of phytoplankton in shear (Bearon *et al.*, 2011). This led us to develop an alternative analytic model that shows excellent agreement with numerical results.

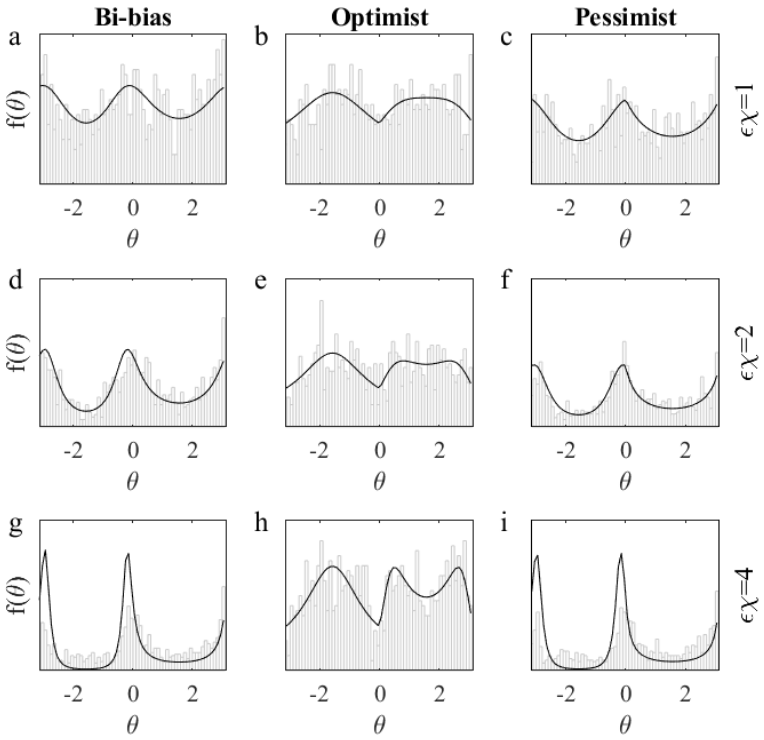

FIG. 7. Comparison of equilibrium direction in individual-based stochastic simulations (histogram) with direct equilibrium solution (solid line) for (a,d,g) bi-bias; (b,e,h) optimist ; (c,f,i) pessimist. Chemotactic strength: (a,b,c) $\varepsilon\chi = 1$; (d,e,f) $\varepsilon\chi = 2$; (g,h,i) $\varepsilon\chi = 4$.

Bacteria generate chemotaxis using a diversity of different mechanisms. While the optimistic strategy of swimming *E. coli* is well known (Berg & Brown, 1972; Berg, 2004), recent experiments suggest that freely swimming *P. aeruginosa* cells might use a similar strategy (Cai *et al.*, 2016). In the absence of serine singly flagellated *P. aeruginosa* reverse direction every 0.56 s, compared to 0.68 s and 0.54 s when swimming up and down a serine gradient, respectively, suggesting a predominately optimistic response. Further experiments are needed, however, to ascertain whether a homogeneous distribution of serine affects the reorientation rate of swimming *P. aeruginosa*, as observed for swimming *E. coli* (Brown & Berg, 1974). Tentatively, though it appears that *P. aeruginosa* might use a pessimistic strategy for pili based chemotaxis (Oliveira *et al.*, 2016) and an optimistic strategy for flagella based chemotaxis (Cai *et al.*, 2016). We note that *P. aeruginosa* uses two distinct molecular systems to regulate pili based and flagella based chemotaxis (Sampedro *et al.*, 2015), such that each could potentially facilitate a different chemotactic strategy.

While the literature contains relatively few measurements of the reorientation rate of bacteria freely swimming in chemical gradients, another way of probing a swimming cell's chemosensory system is to tether the cell to a surface by a single flagellum. In such experiments the cell body rotates, rather than the flagella, allowing one to easily quantify changes in the direction of rotation as the concentration of chemoeffectors flowing past them changes over time. This technique allows a single cell to be observed for long periods. However, these types of assays often expose cells to temporal chemical gradients that are typically much larger than a freely swimming cell would experience in nature (Berg, 2004), thus they are often used to quantify adaptation of the chemosensory system (Block *et al.*, 1983), rather than to probe specific chemotaxis strategies. With this caveat in mind, it appears that *Bacillus subtilis* responds to relatively weak increases in chemoattractant (asparagine) concentrations by extending runs, but similar decreases in chemoattractant concentration produce no measurable response (Kirby *et al.*, 2000). This suggests that swimming *B. subtilis*, which like *E. coli* possesses multiple flagella and performs run-tumble chemotaxis, also employs an optimistic response to generate chemotaxis. While an optimistic response remains to be verified in free-swimming *B. subtilis*, this finding is interesting because the molecular systems that regulate chemotaxis in *B. subtilis* and *E. coli* have major structural differences (Garrity & Ordal, 1995).

Swimming bacteria do not appear, however, to universally use an optimistic strategy to generate chemotaxis. The phytosynthetic bacterium *Rhodobacter sphaeroides* uses a single flagellum to navigate chemical gradients and possesses a comparatively complex signal transduction system, with multiple homologues of the set of chemosensory proteins within *E. coli* (Wadhams & Armitage, 2004; Porter *et al.*, 2008). Interestingly, *R. sphaeroides*'s single flagellum rotates only in one direction and chemotaxis generated using a 'run-stop' behaviour, where stopped cells slowly change their orientation before resuming another run. Tethered cell assays suggest that the main way that *R. sphaeroides* climbs gradient is by increasing its probability of stopping when moving down chemoattractant gradient, which is indicative of a pessimistic response (Packer *et al.*, 1996). This species exhibits a similar response to the reduction in light intensity, which also allows it to perform phototaxis (Berry & Armitage, 2000).

Taken in whole, it tentatively appears that three major models of swimming bacterial chemotaxis, *E. coli*, *P. aeruginosa*, and *B. subtilis*, sharply change their swimming direction using an optimistic strategy, whilst *R. sphaeroides* employs a strategy pessimistic strategy to regulate when it stops. In contrast, surface attached *P. aeruginosa* biofilm cells chemotax using a pessimistic strategy to regulate reversals in their movement direction (Oliveira *et al.*, 2016).

Our model reveals the inherent trade-offs of different chemotaxis strategies and suggest how characteristics of the nutrient environment might select how bacteria regulate their movement. Our results show that an optimistic chemotactic response allows a population to generate both a larger chemotac-

tic drift and larger diffusivity compared with those that employ a pessimistic response. We therefore posit that an optimistic strategy is favoured in highly dynamic environments where there are significant benefits to rapidly find and exploit transient nutrient patches before they dissipate (Taylor & Stocker, 2012; Grünbaum, 2002). Conversely, we find that pessimistic cells can more tightly aggregate where the concentration of nutrients is largest because this strategy allows chemotactic drift to dominate cell diffusion. We propose that pessimistic strategies are favoured in more stable environments where nutrient gradients are long lived, such that cells that can better maintain their position where nutrients are most abundant will have an advantage.

The predictions from our model are in general agreement with empirical observations. Swimming cells are exposed to highly dynamic nutrient landscapes because localized hotspots of a nutrient are rapidly dissipated by molecular diffusion and fluid flow (Fig. 8a, Taylor & Stocker (2012)). This suggests that swimming cells would benefit from an optimistic strategy because it better equips them to find and climb chemical gradients before they dissipate, owing to their larger diffusion and chemotactic drift than pessimistic cells. In contrast, biofilms generate very thin and stable nutrient gradients because nutrient diffusion and consumption balance one another at the surface of a biofilm, such that only the cells at outer edge of a biofilm are metabolically active (Fig. 8b). For example, it has been found that only cells on the outside $\approx 50\mu m$ of *P. aeruginosa* biofilms are actively respiring (Werner *et al.*, 2004). Thus, the distribution of nutrients within a biofilm would exert a strong selection pressure for cells that can maintain their position within this thin nutrient boundary layer, suggesting that biofilm cells might benefit from a pessimistic chemotactic strategy. While the chemotactic strategies of relatively few species has been quantified thus far, it is intriguing that swimming bacteria appear to largely adopt an optimistic strategy (Berg & Brown, 1972; Kirby *et al.*, 2000; Berg, 2004), whilst biofilm cells appear to use a pessimistic strategy (Oliveira *et al.*, 2016).

Bacteria use a variety of different mechanisms to change their direction: our model can be used to understand how these differentially affect population level statistics. Species with multiple flagella often exhibit run and tumble behaviour, but with some degree of correlation in the direction between subsequent runs (Berg & Brown, 1972). In contrast, pili based motility and cells that swim with only one flagella typically exhibit run-reverse behaviour (Cai *et al.*, 2016; Oliveira *et al.*, 2016). Here we parameterize these different reorientation strategies using positive and negative values of persistence, respectively. Our results indicate that run-reverse behaviour of biofilm cells may offer an advantage over run-tumble behaviour because they can tightly aggregate where the nutrients are most abundant. This is because negative persistence reduces the diffusivity but does not alter the chemotactic drift. Future studies many also be able to extend the framework presented here to shed additional light how the run-stop behaviour employed by *R. sphaeroides* or the 'flick' behaviour exhibited by *Vibrio alginolyticus*, which generates 90 degree turns (Son *et al.*, 2016), affects their population level statistics.

Bacteria exhibit a very wide range of motility speeds: marine bacteria have been observed to swim at much faster speeds than enteric bacteria, which in turn move three orders of magnitude faster than biofilm bacteria (Stocker *et al.*, 2008; Oliveira *et al.*, 2016). In this study, we have made an initial attempt to explore how speed affects chemotaxis. We have shown that, when diffusivity is a function of the magnitude of the chemical gradient, the chemotactic accumulation is a non-linear function of speed and it depends on the bacterial strategy, but this behaviour cannot be explained using current linear models of chemotaxis. Recent experiments have demonstrated that chemotactic accumulation is speed dependent and this occurs due to an interesting correlation between reorientation frequency and swimming speed (Son *et al.*, 2016). The mathematical framework presented here could provide further insight into the link between individual-level behaviour and chemotactic accumulation. We have also

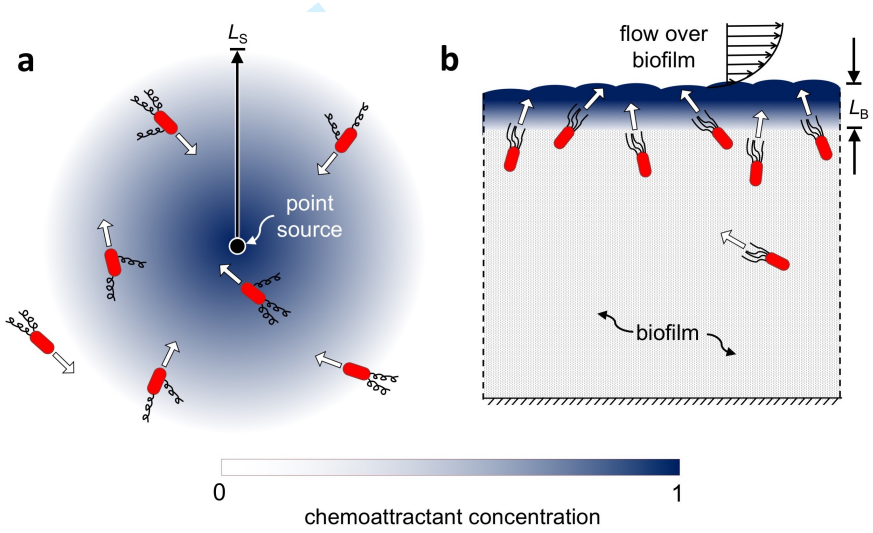

FIG. 8. Swimming and biofilm bacteria experience markedly different chemical gradients in their respective habitats, which may select for disparate chemotactic strategies. (a) Swimming cells navigate along transient gradients of chemicals that freely diffuse through liquids. In the absence of flow, a point source of a chemoattractant (e.g. a lysing phytoplankton cell Smirga *et al.* (2016)) will create a distribution that continuously increases in size like $L_S \approx (D_M \tau)^{1/2}$, where D_M is the molecular diffusion coefficient of the chemoattractant (order $10^{-9} m^2 s^{-1}$ for small molecules), and τ is the elapsed time. However, in practice the distribution of chemoattractant is typically stirred by fluid flow, which tends to sharpen gradients making them more susceptible to irreversible mixing by molecular diffusion (Taylor & Stocker, 2012). Swimming cells must therefore accumulate in ephemeral chemoattractant sources before they are dissipated by mixing, which likely favours chemotactic strategies that confer the ability to rapidly traverse gradients (Taylor & Stocker, 2012; Grünbaum, 2002). (b) Biofilm cells live in densely packed assemblages where limiting nutrients diffuse through the fluid-biofilm interface, where they are immediately consumed. A balance between diffusion and consumption thus generates steep and stable chemical gradients with thickness $L_B \approx \sqrt{c_0 D_B Y \alpha^{-1}}$, where c_0 is the chemoattractant concentration at biofilm's surface, D_B is the diffusion coefficient of the chemoattractant in the biofilm, α is the bacterial growth rate, and Y the yield with which cells convert the nutrient to biomass (Pirt, 1967; Coyte *et al.*, 2017). The thickness of this chemical boundary layer is $L_B \approx 50\mu$m, and typically cells beneath this thin layer cells are not metabolically active (Werner *et al.*, 2004). We posit that the nutrient landscape within biofilms favours chemotactic strategies that allow cells to tightly aggregate within this thin and stable nutrient boundary layer.

demonstrated how the framework can be extended to capture orthotaxis recently observed in surface attached *P. aeruginosa*, although in this context orthotaxis appears to contribute less to the drift of cells along gradients when compared to the chemotactic drift driven by modulation of their reversal rate.

There are many possible additional extensions to the mathematical framework presented here. First, our chemotactic model does not explicitly incorporate temporal integration of the chemical signal, nor have we included the effects of Brownian rotational diffusion. Both are considered by Locsei (2007) who demonstrated that even for a weak chemotactic response, persistence can impact the chemotactic drift, which is an effect not observed in our model. Second, while the signal transduction systems that regulate chemotaxis have been characterised for only a few species, an explicit model of these pathways (e.g. Xue, 2015; Erban & Othmer, 2005; Xue & Yang, 2016) could be integrated into our model of strong chemotaxis to shed additional light how regulatory systems have evolved to optimise behaviour. Third, in this study we posit the spatio-temporal dynamics of the chemoattractant field within a bacteria's environment may shape its chemotactic strategy, but it would be interesting to directly couple the governing equations that describe distributions of cell position and orientation with those that describe the transport of the chemoaffectors (Hein *et al.*, 2016; Taylor & Stocker, 2012). Such a coupled model might facilitate deeper understanding of how different chemical landscapes select for different chemotactic strategies. Fourth, the movement of both swimming and biofilm bacteria can be affected by flow (Bearon, 2003; Bearon & Hazel, 2015; Locsei & Pedley, 2009; Shen *et al.*, 2012), which may also exert an additional selection pressure for cells to co-opt a particular movement strategy. Future studies may be able to determine how chemotactic drift and diffusion are affected by the reorienting effects of fluid shear.

In conclusion, this study reveals the trade-offs of different chemotactic strategies, providing a new framework through which to interpret empirical observations. Many previous studies have focused on how the chemotactic response of *E. coli* optimizes nutrient acquisition (e.g. Celani & Vergassola, 2010; Kollmann *et al.*, 2005), but bacteria possess different forms of motility and live in many diverse environments which have the potential to select for a variety of different behaviours. Technological advances, such as microfluidic experiments (Cai *et al.*, 2016; Oliveira *et al.*, 2016) and holographic microscopy (Molaei *et al.*, 2014), hold significant promise to rapidly quantify the strategies that mediate bacterial chemotaxis in different genotypes, allowing us to expand our knowledge beyond just a few model species. Such comparative studies, when combined with mathematical models like that presented here, may ultimately allow us to resolve unifying principles that diverse species of bacteria use to exploit their habitats. Understanding the fundamental processes that structure bacterial communities has the potential to shed new light on how these communities function in nature, medicine, and industry, as well as potentially give us new tools to manipulate them to our advantage.

Acknowledgements: We thank Judy Armitage, Howard Berg, Thomas Hillen, George Ordal, and Roman Stocker for discussions. We also thank the support from the COST Action MP1305: Flowing matter, with particular mention to the discussions held during the workshop 'Microorganisms in Turbulent Flows', Lorentz Centre, Leiden, the Netherlands. This work is also supported by EPSRC EP/N014499/1 'EPSRC Centre for New Mathematical Sciences Capabilities for Healthcare Technologies' and a starting grant from the University of Sheffield's 'Imagine: Imagining Life' initiative.

References

ADLER, J. 1966 Chemotaxis in bacteria. *Science* **153** (3737), 708–716.

AHMED, T. & STOCKER, R. 2008 Experimental verification of the behavioral foundation of bacterial

transport parameters using microfluidics. *Biophys. J.* **95** (9), 4481 – 4493.

ALT, W. 1980 Biased random-walk models for chemotaxis and related diffusion approximations. *J. Math. Biol.* **9** (2), 147 – 177.

ATKINSON, K. E. & SHAMPINE, L. F. 2008 Solving Fredholm integral equations of the second kind in Matlab. *ACM Trans. Math. Software* **34** (4), 477–496.

BEARON, R.N. & HAZEL, A.L. 2015 The trapping in high-shear regions of slender bacteria undergoing chemotaxis in a channel. *J. Fluid Mech.* **771**.

BEARON, R. N. 2003 An extension of generalized Taylor dispersion in unbounded homogeneous shear flows to run-and-tumble chemotactic bacteria. *Phys. Fluids* **15** (6), 1552 – 1563.

BEARON, R. N. & GRÜNBAUM, D. 2008 From individual behaviour to population models: A case study using swimming algae. *J. Theor. Biol.* **251** (4), 679 – 697.

BEARON, R. N., HAZEL, A. L. & THORN, G. J. 2011 The spatial distribution of gyrotactic swimming micro-organisms in laminar flow fields. *J. Fluid Mech.* **680**, 602–635.

BERG, H. C. 2004 *E. coli in Motion*, 1st edn. Springer New York.

BERG, H. C. & BROWN, D. A. 1972 Chemotaxis in *Escherichia coli* analyzed by 3-Dimensional tracking. *Nature* **239** (5374), 500 – 504.

BERRY, R. M. & ARMITAGE, J. P. 2000 Response Kinetics of Tethered *Rhodobacter sphaeroides* to Changes in Light Intensity. *Biophys. J.* **78**, 1207–1215.

BLOCK, S. M., SEGALL, J. E. & BERG, H. C. 1983 Adaptation kinetics in bacterial chemotaxis. *J. Bacteriol.* **154**, 312–323.

BROWN, D. A. & BERG, H. C. 1974 Temporal stimulation of chemotaxis in *Escherichia coli*. *Proc. Nat. Acad. Sci. USA* **71** (4), 1388–1392.

BUTLER, S. M. & CAMILI, A. 2005 Going against the grain: chemotaxis and infection in *Vibrio cholera*. *Nature Rev. Microbiol.* **3**, 611–620.

CAI, Q., LI, Z., OUYANG, Q., LUO, C. & GORDON, V. D. 2016 Singly flagellated *Pseudomonas aeruginosa* chemotaxes efficiently by unbiased motor regulation. *mBio* **7** (2).

CELANI, A. & VERGASSOLA, M. 2010 Bacterial strategies for chemotaxis response. *Proc. Nat. Acad. Sci. USA* **107**, 1391–1396.

CODLING, E. A., BEARON, R. N. & THORN, G. J. 2010 Diffusion about the mean drift location in a biased random walk. *Ecology* **91** (10), 3106–3113.

COSTERTON, J. W., LEWANDOWSKI, Z., CALDWELL, D. E., KORBER, D. R. & LAPPIN-SCOTT, H. M. 1995 Microbial biofilms. *Ann. Rev. Microbiol.* **49**, 711–745.

COYTE, K. Z., TABUTEAU, H., GAFFNEY, E. A., FOSTER, K. R. & DURHAM, W. M. 2017 Microbial competition in porous environments can select against rapid biofilm growth. *Proc. Nat. Acad. Sci. USA* **114**, E161–E170.

ERBAN, R. & OTHMER, H. G. 2005 From signal transduction to spatial pattern formation in E. coli: a paradigm for multiscale modeling in biology. *Multiscale Model. Simul.* **3**, 362–394.

GARRITY, L. F. & ORDAL, G. W. 1995 Chemotaxis in *Bacillus subtilis*: how bacteria monitor environmental signals. *Pharmacol. Ther.* **68**, 87–104.

GRÜNBAUM, D. 2002 Predicting availability to consumers of spatially and temporally variable resources. *Hydrobiologia* **480** (1-3), 175 – 191.

HEIN, A. M., BRUMLEY, D. R., CARRARA, F., STOCKER, R. & LEVIN, S. A. 2016 Physical limits on bacterial navigation in dynamic environments. *J. Roy. Soc. Interf.* **13**, 20150844.

HILLEN, T. 2006 M^5, Mesoscopic and Macroscopic Models for Mesenchymal Motion. *J. Math. Biol.* **53** (4), 585–616.

HILLEN, T. & OTHMER, H. G. 2000 The diffusion limit of transport equations derived from velocity-jump processes. *SIAM J. Appl. Math.* **61** (3), 751 – 775.

HILLEN, T. & PAINTER, K. 2013 Transport Models for Movement in Oriented Habitats and Anisotropic Diffusion. In *Dispersal, individual movement and spatial ecology: a mathematical perspective* (ed. Lewis, MA and Maini, PK and Petrovskii, SV), *Lecture Notes in Mathematics*, vol. 2071, pp. 177–222.

HILLEN, T. & PAINTER, K. J. 2009 A user's guide to PDE models for chemotaxis. *J. Math. Biol.* **58** (1-2), 183–217.

KEARNS, D. B., ROBINSON, J. & SHIMKETS, L. J. 2001 *Pseudomonas aeruginosa* exhibits directed twitching motility up phosphatidylethanolamine gradients. *J. Bacteriol.* **183**, 763767.

KELLER, E. F. & SEGEL, L. A. 1971 Model for chemotaxis. *J. Theor. Biol.* **30** (2), 225–&.

KIM, M., BIRD, J. C., VAN PARYS, A. J., BREUER, K. S. & POWERS, T. R. 2003 A macroscopic scale model of bacterial flagellar bundling. *Proc. Nat. Acad. Sci. USA* **100**, 1548115485.

KIRBY, J. R., NIEWOLD, T. B., MALOY, S. & ORDAL, G. W. 2000 CheB is required for behavioural responses to negative stimuli during chemotaxis in Bacillus subtilis. *Molecular Microbiol.* **35** (1), 44–57.

KOLLMANN, M., LØVDOK, L., BARTHOLOME, K., TIMMER, J. & SOURJIK, V. 2005 Design principles of a bacterial signalling network. *Nature* **438**, 504–507.

LEAL, L. G. 2007 *Advanced Transport Phenomena*, 1st edn. Cambridge University Press.

LOCSEI, J.T. 2007 Persistence of direction increases the drift velocity of run and tumble chemotaxis . *J. Math. Biol.* **55**, 1432–1416.

LOCSEI, J. T. & PEDLEY, T. J. 2009 Run and tumble chemotaxis in a shear flow: The effect of temporal comparisons, persistence, rotational diffusion, and cell shape. *Bull. Math. Biol.* **71**, 1089–1116.

LOVELY, P. S. & DAHLQUIST, F. W. 1975 Statistical measures of bacterial motility and chemotaxis. *J. Theor. Biol.* **50** (2), 477–496.

MOLAEI, M., BARRY, M., STOCKER, R. & SHENG, J. 2014 Failed Escape: Solid Surfaces Prevent Tumbling of Escherichia coli. *Phys. Rev. Letts.* **113**, 068103.

OLIVEIRA, N. M., FOSTER, K. R. & DURHAM, W. M. 2016 Single-cell twitching chemotaxis in developing biofilms. *Proc. Nat. Acad. Sci. USA* **113** (23), 6532–6537.

OTHMER, H. G. & XUE, C. 2013 The Mathematical Analysis of Biological Aggregation and Dispersal: Progress, Problems and Perspectives. In *Dispersal, individual movement and spatial ecology: a mathematical perspective* (ed. Lewis, MA and Maini, PK and Petrovskii, SV), *Lecture Notes in Mathematics*, vol. 2071, pp. 79–127.

PACKER, H. L., GAUDEN, D. E. & ARMITAGE, J. P. 1996 The behavioural response of anaerobic *Rhodobacter sphaeroides* to temporal stimuli. *Microbiol.* **142**, 593–599.

PANDEY, G. & JAIN, R. K. 2002 Bacterial chemotaxis toward environmental pollutants: Role in Bioremediation . *Appl. Environmental Microbiol.* **68**, 57895795.

PIRT, S 1967 A kinetic study of the mode of growth of surface colonies of bacteria and fungi. *J. Gen. Microbiol.* **42**, 181–197.

PORTER, S. L., WADHAMS, G. H. & ARMITAGE, J. P. 2008 Rhodobacter sphaeroides: complexity in chemotactic signalling. *Trends. Microbiol.* **16** (6), 251–260.

RIVERO, M. A., TRANQUILLO, R. T., BUETTNER, H. M. & LAUFFENBURGER, D. A. 1989 Transport models for chemotactic cell-populations based on individual cell behavior. *Chem. Eng. Sci.* **44** (12), 2881 – 2897.

SAINTILLAN, D. & SHELLEY, M. J. 2013 Active suspensions and their nonlinear models. *Comptes Rendus Physique* **14** (6), 497–517.

SAMPEDRO, I., PARALES, R. E., KRELL, T. & HILL, J. E. 2015 *Pseudomonas* chemotaxis. *FEMS Microbiol. Rev.* **39**, 17–46.

SHEN, Y., SIRYAPORN, A., LECUYER, S., GITAI, Z. & STONE, H. A. 2012 Flow directs surface-attached bacteria to twitch upstream. *Biophys. J.* **103** (1), 146–151.

SKERKER, J. M. & BERG, H. C. 2001 Direct observation of extension and retraction of type IV pili . *Proc. Nat. Acad. Sci. USA* **98**, 6901–6904.

SMIRGA, S., FERNANDEZ, V. I., MITCHELL, J. G. & STOCKER, R. 2016 Chemotaxis toward phytoplankton drives organic matter partitioning among marine bacteria. *Proc. Nat. Acad. Sci. USA* **113**, 15761581.

SON, K., MENOLASCINA, F. & STOCKER, R. 2016 Speed-dependent chemotactic precision in marine bacteria. *Proc. Nat. Acad. Sci. USA* **113** (31), 8624–8629.

STOCKER, R., SEYMOUR, J. R., SAMADANI, A., HUNT, D. E. & POLZ, M. F. 2008 Rapid chemotactic response enables marine bacteria to exploit ephemeral microscale nutrient patches. *Proc. Nat. Acad. Sci. USA* **105** (11), 4209 – 4214.

TAYLOR, J. R. & STOCKER, R. 2012 Trade-offs of chemotactic foraging in turbulent water. *Science* **338** (6107), 675–679.

TAYLOR-KING, J. P., VAN LOON, E. E., ROSSER, G. & CHAPMAN, S. J. 2015 From Birds to Bacteria: Generalised Velocity Jump Processes with Resting States. *Bull. Math. Biol.* **77** (7), 1213–1236.

THYGESEN, U. H. 2016 A diffusion approximation based on renewal processes with applications to strongly biased run-tumble motion. *Bull. Math. Biol.* **78**, 556–579.

TINDALL, M. J., MAINI, P. K., PORTER, S. L. & ARMITAGE, J. P. 2008 Overview of mathematical approaches used to model bacterial chemotaxis II: Bacterial populations. *Bull. Math. Biol.* **70**, 1570–1607.

WADHAMS, G. H. & ARMITAGE, J. P. 2004 Making sense of it all: bacterial chemotaxis. *Nature Reviews Microbiology* **5**, 1024–1037.

WERNER, E., ROE, F., BUGNICOURT, A., FRANKLIN, M. J., HEYDORN, A., MOLIN, S., PITTS, B. & STEWART, P. S. 2004 Stratified growth in *Pseudomonas aeruginosa* biofilms. *Appl. Environmental Microbiol.* **70**, 61886196.

XUE, C 2015 Macroscopic equations for bacterial chemotaxis: integration of detailed biochemistry of cell signaling . *J. Math. Biol.* **70**, 1–44.

XUE, C. & YANG, X. 2016 Moment-flux models for bacterial chemotaxis in large signal gradients. *J. Math. Biol.* **73**, 977–1000.

A. Expansion solution for ψ

To obtain the leading order solution for $\psi^{(0)}$ for weak chemotaxis, we consider a Fourier series expansion (Hillen & Othmer, 2000):

$$\psi^{(0)} = \sum_k a_k^{(0)}(y,t)\cos k\theta + b_k^{(0)}(y,t)\sin k\theta, \tag{A.1}$$

and consider the class of turn kernels, $K(\theta,\theta') = h(|\theta-\theta'|)$, where h is a sufficiently smooth function. We define the following moments of the turn kernel:

$$\alpha_k = 2\int_0^\pi \cos(ku)h(u)du, \tag{A.2}$$

noting that $\alpha = \alpha_1$ is the index of persistence as defined as the mean cosine of the turn angle (Lovely & Dahlquist, 1975; Othmer & Xue, 2013). If tumbles reorientate cells randomly, such that their new swimming direction is uncorrelated to their previous one, the index of persistence is zero. In contrast, if tumbles change a cell's swimming direction only slightly, so that they move in nearly the same direction after tumbling, the index of persistence would tend towards one.

From equation (2.26), using standard trigonmetric identities, periodicity and noting $\sin(ku)h(|u|)$ is an antisymmetric function which will integrate to zero, we obtain the result that

$$\begin{aligned}\sum_k a_k^{(0)}(y,t)\cos k\theta + b_k^{(0)}(y,t)\sin k\theta &= \int_{-\pi}^{\pi} h(|\theta-\theta'|)\left(\sum_k a_k^{(0)}(y,t)\cos k\theta' + b_k^{(0)}(y,t)\sin k\theta'\right)d\theta', \\ &= \sum_k \alpha_k\left(a_k^{(0)}(y,t)\cos k\theta + b_k^{(0)}(y,t)\sin k\theta\right).\end{aligned}$$

As $\alpha_0 = 1$, the θ independent ($k = 0$) terms agree. For $k > 0$, provided $\alpha_k \neq 1$ (corresponding to a cells which changes its movement direction), we obtain the result that $a_k(y,t) = b_k(y,t) = 0$. We therefore obtain the solution

$$\psi^{(0)}(y,\theta,t) = a_0(y,t). \tag{A.3}$$

As we define $n^{(0)}(y,t) = \int_{-\pi}^{\pi} \psi^{(0)}(y,\theta,t)d\theta$, we thus obtain the required result:

$$\psi^{(0)}(y,\theta,t) = \frac{1}{2\pi} n^{(0)}(y,t). \tag{A.4}$$

For strong chemotaxis, we consider the following expression for $\psi^{(0)}$:

$$\psi^{(0)} = f(\theta)\left(\sum_k c_k^{(0)}(z,t)\cos k\theta + d_k^{(0)}(z,t)\sin k\theta\right), \tag{A.5}$$

where f is the steady distribution given by equation (2.36). Inserting this expansion into equation (2.43) we obtain:

$$\begin{aligned}\sum_k c_k^{(0)}(z,t)\cos k\theta + d_k^{(0)}(z,t)\sin k\theta &= \int_{-\pi}^{\pi} h(|\theta-\theta'|)\left(\sum_k c_k^{(0)}(z,t)\cos k\theta' + d_k^{(0)}(z,t)\sin k\theta'\right)d\theta', \\ &= \sum_k \alpha_k\left(c_k^{(0)}(z,t)\cos k\theta + d_k^{(0)}(z,t)\sin k\theta\right).\end{aligned}$$

As for the weak chemotaxis case, for cells which undergo changes in direction, we obtain the result that for $k > 0$, $c_k^{(0)}(y,t) = d_k^{(0)}(y,t) = 0$ and hence

$$\psi^{(0)}(z,\theta,t) = f(\theta)n^{(0)}(z,t). \tag{A.6}$$

To obtain the solution for $\psi^{(1)}$, we propose the following expression for $\lambda(\theta)\psi^{(1)}(z,\theta,t)$:

$$\lambda(\theta)\psi^{(1)} = -\lambda(\theta)f^{(1)}(\theta)\frac{\partial n^{(0)}}{\partial z} + \sum_k c_k^{(1)}(z,t)\cos k\theta + d_k^{(1)}(z,t)\sin k\theta. \tag{A.7}$$

where $f^{(1)}(\theta)$ is a smooth periodic function which satifies equations (2.47, 2.48).

Inserting this expansion into equation (2.45) yields

$$\begin{aligned}\sum_k c_k^{(1)}(z,t)\cos k\theta + d_k^{(1)}(z,t)\sin k\theta &= \int_{-\pi}^{\pi} h(|\theta-\theta'|)\left(\sum_k c_k^{(1)}(z,t)\cos k\theta' + d_k^{(1)}(z,t)\sin k\theta'\right)d\theta', \\ &= \sum_k \alpha_k\left(c_k^{(1)}(z,t)\cos k\theta + d_k^{(1)}(z,t)\sin k\theta\right).\end{aligned}$$

As in the previous calculations, for cells which undergo changes in direction, that is for $k > 0$, $\alpha_k \neq 1$, we obtain the result that for $k > 0$, $c_k^{(1)}(y,t) = d_k^{(1)}(y,t) = 0$. On taking the first moment of $\psi^{(1)}$ we obtain the expression

$$n^{(1)}(z,t) = \int_{-\pi}^{\pi} \psi^{(1)} d\theta = -\frac{\partial n^{(0)}}{\partial z}\int_{-\pi}^{\pi} f^{(1)}(\theta)d\theta + c_0^{(1)}\int_{-\pi}^{\pi}\frac{1}{\lambda}d\theta. \tag{A.8}$$

Using equation (2.48), we thus obtain the following expression for $c_0^{(1)}$:

$$c_0^{(1)} = \frac{n^{(1)}}{\int_{-\pi}^{\pi} \frac{1}{\lambda(\theta)} d\theta}. \tag{A.9}$$

From equation (A.7), we hence obtain the required result that

$$\psi^{(1)} = -f^{(1)}(\theta)\frac{\partial n^{(0)}}{\partial z} + f(\theta)n^{(1)} \tag{A.10}$$

where f is the steady distribution given by equation (2.36).

B. Derivation of moment equations

We here explain how to obtain equations (2.23, 2.24) which relate the first three moments of ψ: $n(y,t) = \int_{-\pi}^{\pi} \psi(y,\theta,t)d\theta$, $j(y,t) = \int_{-\pi}^{\pi} \sin\theta\psi d\theta$ and $Q(y,t) = \int_{-\pi}^{\pi} \sin^2\theta\psi d\theta$, in the case of weak chemotaxis.

We first consider the non-dimensional conservation equation for ψ for weak chemotactic response, equation (2.19):

$$\begin{aligned} \varepsilon^2\frac{\partial \psi}{\partial t} &+ \varepsilon\frac{\partial}{\partial y}(\sin\theta\psi) + (1-\varepsilon\chi\sin\theta)\psi \\ &- \int_{-\pi}^{\pi}(1-\varepsilon\chi\sin\theta')K(\theta,\theta')\psi(\theta')d\theta' = 0. \end{aligned}$$

The zero moment, that is integrating this equation over θ, gives equation (2.23):

$$\varepsilon^2\frac{\partial n}{\partial t} + \varepsilon\frac{\partial j}{\partial y} = 0.$$

Here we used the result that $\int_{-\pi}^{\pi} K(\theta,\theta')d\theta = 1$, i.e. after tumbling a cell must move in some direction, to eliminate the tumble terms.

To obtain the first moment, equation (2.24), requires some intermediary calculations similarly to that found in the above appendix A. Specifically, we can obtain the result that for turn kernels of the form $K(\theta,\theta') = h(|\theta-\theta'|)$, we have that

$$\int_{-\pi}^{\pi} \sin\theta K(\theta,\theta')d\theta = \sin\theta'\alpha. \tag{B.1}$$

where α is the index of persistence as defined by α_1 in equation (A.2). The first moment, that is integrating equation (2.19) multiplied by $\sin\theta$ over θ thus gives equation (2.24):

$$\varepsilon^2\frac{\partial j}{\partial t} + \varepsilon\frac{\partial Q}{\partial y} + (1-\alpha)j - \varepsilon(1-\alpha)\chi Q = 0. \tag{B.2}$$

C. Calculation of $f^{(1)}$

Equation (2.47) is a Fredholm integral equation of the second kind for the composite function $\lambda f^{(1)}$. The equation only specifies $\lambda f^{(1)}$ up to an arbitrary constant, as $\int_{-\pi}^{\pi} K(\theta,\theta')d\theta' = 1$. The arbitrary

constant is found by specifying $\int_{-\pi}^{\pi} f^{(1)} d\theta = 0$. In the case of isotropic tumbles, the solution can be found analytically and is discussed in section 3.2. For more general expressions for the turn kernel, numerical methods were used. Specifically, we used a composite left one-point quadrature method with uniform subintervals to obtain an initial estimate for $\lambda \tilde{f}^1$, and then chose a suitable normalisation constant C_1 to ensure $\int f^{(1)} d\theta = 0$:

$$f^1 = \frac{\lambda \tilde{f}^1 + C_1}{\lambda}. \tag{C.1}$$

Implementation in Matlab was based on Atkinson & Shampine (2008). To verify this numerical scheme we compared with the analytic results obtained for isotropic tumbles and found the results were indistinguishable with a uniform grid for θ of size 512.